The Neoarchaean Storø Supracrustal Belt, Nuuk region, southern West Greenland : an arc-related basin with continent-derived sedimentation

Szilas, K; van Gool, J.A.M.; Scherstén, Anders; Frei, R

Published in:
Precambrian Research

DOI:
10.1016/j.precamres.2014.04.010

2014

Title: The Mesoarchaean Storø Supracrustal Belt, Nuuk region, southern West Greenland: An arc-related basin with continent-derived sedimentation

Author: Kristoffer Szilas Jeroen A.M. van Gool Anders Scherstén Robert Frei

PII: S0301-9268(14)00129-6
DOI: http://dx.doi.org/doi:10.1016/j.precamres.2014.04.010
Reference: PRECAM 3968

To appear in: *Precambrian Research*

Received date: 24-6-2013
Revised date: 25-1-2014
Accepted date: 10-4-2014

Please cite this article as: Szilas, K., van Gool, J.A.M., Scherstén, A., Frei, R.,The Mesoarchaean Storo Supracrustal Belt, Nuuk region, southern West Greenland: An arc-related basin with continent-derived sedimentation, *Precambrian Research* (2014), http://dx.doi.org/10.1016/j.precamres.2014.04.010

The Mesoarchaean Storø Supracrustal Belt, Nuuk region, southern West Greenland: An arc-related basin with continent-derived sedimentation

Kristoffer Szilas [a, b, *], Jeroen A.M. van Gool [a, c], Anders Scherstén [a, d], Robert Frei [e]

[a] Geological Survey of Denmark and Greenland (GEUS), Øster Voldgade 10, 1350 Copenhagen K, Denmark

[b] Currently at: Lamont-Doherty Earth Observatory, Columbia University, PO Box 1000, Palisades, NY 10964-8000, USA

[c] Currently at: vG Geoconsult, Glimvej 38, 2650 Hvidovre, Denmark

[d] Currently at: Department of Geology, Lund University Sölvegatan 12, 223 62 Lund, Sweden

[e] Department of Geography and Geology, University of Copenhagen, Øster Voldgade 10, 1350 Copenhagen K, Denmark

* Corresponding author.

E-mail address: kszilas@ldeo.columbia.edu (K. Szilas).

ABSTRACT

We present new major and trace element data, as well as Sm-Nd isotope compositions for Archaean supracrustal rocks and a gabbro-anorthosite complex from the island of Storø in Godthåbsfjord, southern West Greenland. We also provide new U-Pb isotope data for zircon extracted from these rocks. The Storø rocks have experienced amphibolite facies metamorphism, and the entire sequence forms an east-dipping frontal thrust ramp in tectonic contact with Mesoarchaean ('Nûk') gneisses to the west and Eoarchaean ('Itsaq') gneisses to the east. These orthogneisses record a complex regional accretion history, as established by previous work. The present study aims at explaining the geochemical features of the Storø Supracrustal Belt (SSB), which comprises metavolcanic and

metasedimentary rocks that are situated within this collisional zone. The SSB has a maximum age of ca. 2800 Ma, constrained by the youngest detrital zircon population found in a metasedimentary unit. The minimum age of the SSB is 2707 ±8 Ma, defined by previously published Re-Os isotope data. The metavolcanic rocks have a tholeiitic basaltic composition, with generally flat primitive mantle-normalised trace element patterns and generally negative Nb-anomalies (Nb/Nb* 0.30-0.90). They plot above the mantle array in Th/Yb-Nb/Yb space, consistent with a subduction zone affinity, as also proposed by previous studies. A thin fault contact separates the SSB from a gabbro-anorthosite complex (formally defined here as the 'Storø Anorthosite Complex'), which has an age of ca. 3050 Ma. The Sm-Nd isotope data of the SSB suggest, that these metavolcanic rocks experienced contamination by a crustal source that was isotopically similar to the Storø Anorthosite Complex (SAC). This in turn suggests that the SAC could have formed the basement for the younger volcanic sequence of the SSB or alternatively that the mantle source of the SSB was contaminated by melts derived from SAC-aged crust or sediments. The metasedimentary rocks of SSB show a mixed mafic-felsic component with variable degrees of maturity. Highly mature metasediments of the SSB contain several age populations of regionally well-known magmatic events, and thus support a significant local crustal provenance. Furthermore, the youngest documented detrital zircon is found in a thin metasedimentary unit within the metavolcanic rocks, and thereby shows that the SSB formed in close proximity to subaerially exposed continental crust (i.e. a back-arc environment) and not a distal island arc setting as previously proposed. Additionally, this suggests, that relatively cool lower continental crust, which was capable of supporting subaerial mountains, existed at least locally during the Mesoarchaean.

Keywords: Godthåbsfjord; Metasedimentary rocks; Quartzite; Storø Anorthosite Complex; Sm-Nd isotope data

1. Introduction

The petrogenesis of Archaean supracrustal belts is much debated and controversy exists about what type(s) of geodynamic setting was operating during the Archaean. This question has polarized the scientific community into two groups; one favouring uniformitarian principles with subduction and modern-style plate tectonics (e.g. Polat et al., 2002, 2011a; Dilek and Polat, 2008; Friend and Nutman, 2010; Hoffmann et al., 2011a) and another group favouring vertical Archaean tectonics dominated by mantle plumes (e.g. Hamilton, 1998, 2011; Davies, 1999; McCall, 2003; Stern, 2005, 2008; Bédard, 2006). However, there appears to be a growing consensus from recent research that the Archaean supracrustal belts of southern West Greenland points exclusively toward a subduction zone geodynamic environment (Windley and Garde, 2009; Friend and Nutman, 2010; Hoffmann et al., 2011a; Polat et al., 2011a; Szilas et al., 2012a, 2012b, 2013a, 2013b; Furnes et al., 2013; 2014).

In this paper we present new major, trace and isotope data for Archaean supracrustal rocks from the island of Storø in the Nuuk region of southern West Greenland. These rocks have previously been proposed to have formed in a distal oceanic island arc setting (Polat, 2005; Ordóñez-Calderón et al., 2011). Although our data also support a subduction zone affinity, there is geochemical evidence for crustal contamination, which together with the abundance of highly mature clastic sediments point towards a proximal environment (i.e. close to the margin of a continent). Furthermore, we confirm that the amphibolites on Storø represent two distinct age groups, belonging to the Storø Supracrustal Belt (<2800 Ma) and the Storø Anorthosite Complex (ca. 3050 Ma), respectively, as recently proposed by Szilas and Garde (2013). Finally, we provide a broad synthesis of geological background material in **Appendices A and B** in order to contribute with all available information relevant for an up-to-date interpretation of the petrogenesis of the Storø

Supracrustal Belt. This contribution is based in part on the unpublished M.Sc. thesis of K. Szilas (2008) and a report by the Geological Survey of Denmark and Greenland (GEUS) (van Gool et al., 2007).

All of the rocks on Storø have experienced amphibolite facies metamorphism, and thus the prefix 'meta' is taken as implicit for all rock types throughout this paper. Treatment of the Au mineralisation in the Storø supracrustal rocks (Østergaard and van Gool, 2007) is beyond the scope of this paper and we refer the reader to Scherstén et al. (2012) and Kolb et al. (2013) for the latest model about the origin of the Au deposit on Storø. Likewise, we will not discuss the premetamorphic alteration of these rocks, which has recently been covered by Szilas and Garde (2013).

2. Geological background

Below we give a brief description of the geological setting of the Nuuk region with an emphasis on Storø. We also provide an extensive description of the supracrustal rocks on Storø in terms of previous metamorphic, geochronological and structural work, which due to space constraints; can be found in the supplementary **Appendix A**. Much of this information is based on unpublished theses and reports by the Geological Survey of Denmark and Greenland (GEUS), which can be hard to access for the broader scientific community. We therefore make this information readily available via the associated online material.

The island of Storø is located in Godthåbsfjord about 45 km northeast of Nuuk, the capital of Greenland (**Fig. 1**). The supracrustal rocks described here are situated in the central part of Storø. The Nuuk region has recently been subject to geological research and mapping by GEUS and BMP (Bureau of Minerals and Petroleum) (e.g. Hollis et al., 2004, 2006; Hollis, 2005; Stendal, 2007;

Knudsen et al., 2007; van Gool et al., 2007). The map in **Fig. 2** covers the mountains of 'Aappalaartoq' and 'Little Qingaaq' in the central part of Storø. We refer to the latter simply as 'Qingaaq' throughout this paper. Detailed maps of the two mountains are presented in **Appendix C (Figs. C1 and C2)**.

The Nuuk region is dominated by grey gneisses of the tonalite-trondhjemite-granodiorite (TTG) suite, which formed during several episodes of crustal growth (McGregor, 1984; Nutman et al., 1989, 2004; Friend and Nutman, 1991, 2005; Nutman and Friend, 2007). These rocks have experienced amphibolite to granulite facies metamorphism, as well as extensive thrusting and folding (Nutman et al., 2004; Friend and Nutman, 2005).This Archaean crust is part of the North Atlantic craton and can be correlated with the Archaean gneisses of the Nain Province in Labrador, Canada (Bridgewater and Schiøtte, 1991; Wilton, 1994). These orthogneisses represent different crustal terranes, each of which has a separate tectono-metamorphic evolution. The Nuuk region is presently subdivided into several terranes (Friend et al., 1987, 1988, 1996; Nutman et al., 1989; Crowley, 2003). These terranes are thought to have accreted and amalgamated during the Neoarchaean and are separated by crustal-scale tectonic boundaries and narrow shear zones (Nutman and Friend, 2007). However, the Storø shear zone (Fig. 2) represents a smaller scale structure and was developed along the western margin of the Storø supracrustal rocks during metamorphism at ca. 2630 Ma (Hollis, 2005).

Recently a new tectonic model have been proposed for the Nuuk region by Dziggel et al. (2014) in which they propose that these terranes essentially represent paired metamorphic belts, with southwards subduction of the Færingehavn terrane underneath the Tre Brødre and Tasiusarsuaq terranes.

Supracrustal belts (also known as greenstone belts in other parts of the world) are present both within and at the boundaries of the terranes in the Nuuk region. They are generally comprised of

metavolcanic rocks with subordinate metasedimentary lithologies. The Storø supracrustal rocks are located at the margin of the 'Akia' and 'Færingehavn'/'Tre Brødre' terranes and are bounded on both sides by folded shear zones that were active around 2720 Ma (Friend and Nutman, 1991; Nutman and Friend, 2007).

The Storø supracrustal sequence represents a tectonic slice of metavolcanic and metasedimentary rocks, most of which are typical of the Archaean such as mafic to intermediate amphibolites, ultramafic rocks, garnet-mica-sillimanite gneiss and fuchsite-bearing quartzites (Hollis et al., 2004; Knudsen et al., 2007; van Gool et al., 2007; Ordóñez-Calderón et al., 2011). The mafic igneous rocks on Storø (now amphibolites), represents a composite of the ca. 3050 Ma Storø Anorthosite Complex (SAC) and the <2800 Ma volcanic-sedimentary sequence of the Storø Supracrustal Belt (SSB) (Hollis, 2005; Nutman et al., 2007; van Gool et al, 2007; Szilas and Garde, 2013; this study).

The SAC is intruded by a ca. 3050 Ma tonalite sheet (Hollis, 2005). Felsic sheets within the layered amphibolites associated with the anorthosite also yield ages of ca. 3050 Ma (Szilas and Garde, 2013; van Gool et al., 2007), additionally the gabbro associated with the SAC contains zircon with a similar U-Pb age (**Section 5.3**). All of this is taken as evidence for a minimum age of 3050 Ma for the SAC. The maximum age of <2800 Ma for the SSB is defined by the youngest detrital zircon age population in biotite gneisses interpreted as metasediments (Nutman et al., 2007; van Gool et al., 2007; **section 5.3; Appendix A**). A high-strain zone at the boundary between layered amphibolites of the SAC and the <2800 Ma biotite gneiss unit of the SSB, indicates a structural break and marks the contact that separates the two differently aged rock associations (van Gool et al., 2007; Scherstén et al., 2012; Szilas and Garde, 2013; **Appendix A**). However, in the field it is not obvious that there is a tectonic break between the layered amphibolite and the biotite gneiss units, although the rocks show signs of high strain with rotation of porphyroblasts (van Gool et al., 2007; Scherstén et al., 2012; **Appendix A**). In principle this could also represent a non-

conformable contact of sediments deposited on top of older igneous basement. We explore these two possibilities during the discussion of our data (**Section 6.4**).

The youngest events on Storø are represented by the ca. 2550 Ma Qôrqut granitic pegmatites (Nutman et al., 2007, 2010), and Palaeoproterozoic mafic dykes (Kalsbeek et al., 1983), which crosscut all lithological units of the SSB and the SAC (**Fig. 2**).

3. Lithological units and petrography

Appendix B of the online supplementary material provides detailed descriptions of all lithological units present on Storø, as well as detailed petrographic descriptions of specific samples. Therefore we only give a brief summary below of the main features of the different units that form part of the SSB and the SAC, for which we present geochemical data in later sections. The maps found in **Appendix C (Figs. C1 and C2)** were originally prepared at 1:2500-scale by van Gool et al. (2007). We adopt the lithological classification defined in these detailed maps and add the unit class in parenthesis after each rock type throughout this paper. We would like to emphasise that this classification relates to mapable units and is strictly based on the field appearance and mineralogy of the rocks. However, some rock types represent subunits as defined in the field from the presence of specific and spatially confined characteristics as we explain below.

The amphibolite (unit a) is dark, homogeneous, medium-grained and well-foliated (**Fig. 3a**). It contains about 60% modal hornblende, 30% plagioclase, 5% titanite (often as rims around a core of ilmenite) and 5% opaque minerals like ilmenite, magnetite and some minor sulphides (pyrrhotite, chalcopyrite and arsenopyrite). The amphibolite has a well-equilibrated texture and foliation is defined by elongated amphibole, plagioclase and titanite grains. Locally there are garnet-rich areas in the amphibolite unit, which we describe as the garnet amphibolite sub-unit (**Fig. 3b**). These

garnets have almandine composition and biotite is commonly present in this subunit. Such garnet amphibolites may in part be the result of alteration, particularly when associated with biotite, and are therefore treated separately in the geochemical discussion. Within the amphibolite (unit a) there are fragmental, light patches that have been deformed (**Fig. 4**). These have previously been interpreted as being of primary volcaniclastic origin (van Gool et al., 2007).

The garnet-rich gneiss (unit grt) is only found in the contact between the amphibolite (unit a) and the biotite gneiss (unit b) (**Fig. 3c**). In some localities, trains of unaltered and undeformed amphibolite are found within the garnet-rich gneiss showing gradational contacts (Szilas and Garde, 2013). The garnet-rich gneiss is light grey with cm- to dm-size layers of garnet and consists of a varying content of plagioclase, garnet, biotite, quartz, and commonly sillimanite, as well as opaque minerals. The grey matrix consists of plagioclase, biotite and minor quartz. Sillimanite is often found in cm-scale layers as fibrolite around plagioclase- and quartz-rich patches. Garnet can form up to 40% of the rock and is generally evenly distributed, but also occur in biotite-rich bands between more felsic domains, which in places give the rock a layered appearance. Locally sillimanite-rich layers contain rhombic shapes that could represent pseudomorphs after andalusite (van Gool et al., 2007). The rock is poorly foliated by biotite and garnet overgrows this foliation. Garnet shows bell-shaped Mn-zonation, which is consistent with prograde metamorphic growth (Persson, 2007). The mineral assemblage of the garnet-rich gneiss has previously led to the interpretation that this rock originated as a metapelite, but field evidence together with its geochemical features show that it represents a pre-metamorphic alteration product of the basaltic protolith of amphibolite (unit a) (Knudsen et al., 2007; van Gool et al., 2007; Szilas, 2008; Szilas and Garde, 2013).

The calc-silicate gneiss (unit f) is found as bands within the amphibolite unit up to 20 m wide (**Fig. 3d**). This rock has a widely variable content of plagioclase, quartz, hornblende, garnet,

diopside, titanite, chlorite, epidote, carbonates and opaque minerals. It has a layered appearance and is medium-grained, well-foliated and contains cm-sized garnet porphyroblasts. The greenish colour of the rock is due to pale green amphibole, diopside, epidote and chlorite. In places, enclaves of dark amphibolite are observed within the calc-silicate gneiss, and the contacts to the surrounding amphibolite are gradational and irregular, which together with its unusual mineralogy is interpreted as evidence for an origin by alteration from a basaltic precursor prior to metamorphism (van Gool et al., 2007; Szilas, 2008).

The biotite gneiss (unit b) includes a variety of rock types that are all characterised by biotite, plagioclase and quartz (**Fig. 3e**). The garnet content is commonly around 15%, sillimanite mostly comprise less than 5% and cordierite has been observed in a few locations. The transitions within this unit are gradational and compositional layering is seen on scales of decimetres to tens of metres. The biotite gneiss is weakly foliated, despite its high biotite content. In some areas quartzo-feldspathic leucosomes indicate conditions at the beginning of partial melting for this rock. A layer of biotite gneiss about 20 m wide occurs within the amphibolite (unit a) (**Fig. C1**) and U-Pb zircon isotope data are presented for this unit in **Section 5.3** (sample KSZ-06).

Quartzite (unit q) has a grey colour, but weathers orange to light brown (**Fig. 3f**). It is medium-grained, and beside quartz, these rocks contain minor muscovite, and variable small amounts of sillimanite and fuchsite, all of which are heterogeneously distributed throughout the rock. Locally, fuchsite can form up to 20% of the rock. Garnet is rare, but garnet-rich layers commonly contain sillimanite in elongate, square pods, which are potentially pseudomorphs after kyanite. The contact with quartzitic gneiss (unit qmz) is gradual.

Although we only present preliminary data for the Storø Anorthosite Complex (SAC), we briefly present the main characteristics of these rocks below. The anorthosite is homogeneous, medium to coarse grained and massive, consisting of calcic plagioclase with minor hornblende in stringers and

218 along foliation planes. The gabbroic amphibolite (unit ag) that is associated with the anorthosite is
219 medium grained and consists of hornblende and plagioclase in mm to cm scale layering. Plagioclase
220 porphyroclasts occur locally with diameters up to 2 cm. The layered amphibolite (unit av), which is
221 also associated with the SAC, is more heterogeneous and has an overall intermediate composition.
222 It contains felsic layers due to variable proportions of hornblende, feldspar, quartz and biotite.
223 Locally, this rock type is highly strained and contains rotated porphyroblasts of plagioclase.
224
225 **4. Methods**
226
227 Major and trace element analyses were determined by X-Ray Fluorescence spectroscopy (XRF)
228 and Inductively Coupled Plasma Mass Spectrometry (ICP-MS) methods, respectively, at Geological
229 Survey of Denmark and Greenland (GEUS) and exclusively by ICP methods at ACME-labs in
230 Vancouver, Canada. A subset of samples was analysed for their Sm-Nd isotope compositions by
231 Thermal Ionisation Mass Spectrometry (TIMS) at the University of Copenhagen. We have
232 additionally measured U-Pb isotope compositions of zircon by Laser Ablation Inductively Coupled
233 Plasma Mass Spectrometry (LA-ICP-MS) at the GEUS in order to get absolute age constraints for
234 these rocks. Detailed descriptions of the analytical procedures can be found in the online **Appendix**
235 **D**. All data can be found in the supplementary **Tables 1-3**.
236
237 **5. Results**
238
239 Below we present the new the geochemical data for the rocks from Storø. We mainly discuss the
240 geochemical compositions of the lithological units of the Storø Supracrustal Belt (SSB), as they
241 comprise the majority of the mafic igneous sequence on Storø. However, we include all rock units

242 from Storø that we have analysed to provide a complete inventory of the avaiable data for future
243 reference. All major- and trace element data can be found in the supplementary **Table 1**. The Sm-
244 Nd isotopic data can be found in supplementary **Table 2**, and the U-Pb zircon data can be found in
245 supplementary **Table 3**. We present additional geochemical diagrams in **Appendix C**, which we
246 refer to with the prefix 'C'.
247
248 5.1. Major and trace element data
249
250 Amphibolite (unit a) (n = 11) has SiO_2 of 47.1-50.2 wt.%, TiO_2 of 0.74-2.5 wt.% and MgO of
251 5.7-8.8 wt.%. Trace element ranges are: 40-157 ppm Zr, 1.1-7.2 ppm Nb, 17.6-47.2 ppm Y, 20.4-
252 214 ppm Ni and 64.3-356 ppm Cr. Their chondrite-normalised REE pattern are mostly flat with
253 La_{CN}/Sm_{CN} of 0.585-1.57, La_{CN}/Yb_{CN} of 0.475-1.99 and Eu/Eu* [= $Eu_{CN}/\sqrt{(Sm_{CN}xGd_{CN})}$] of 0.83-
254 1.02 (**Fig. C3**). Their primitive-normalised pattern is generally flat, but they have negative Nb-
255 anomalies with Nb/Nb* [= $Nb_{PM}/(\sqrt{(Th_{PM}xLa_{PM})})$] of 0.30-0.90 (**Fig. 5**). Their weathering index
256 according to the classification of Ohta and Arai (2007) range between 4.0-8.1 (**Fig. 6**).
257 Garnet amphibolite (n = 6), a subunit of the above unaltered amphibolites, has SiO_2 of 48.6-53.1
258 wt.%, TiO_2 of 0.99-1.23 wt.% and MgO of 2.04-7.39 wt.%. Trace element ranges are: 46.8-139
259 ppm Zr, 2.47-6.0 ppm Nb, 20.2-42.7 ppm Y, 44.9-156 ppm Ni and 114-232 ppm Cr. Their
260 chondrite-normalised REE pattern are mostly flat, but slightly depleted in LREE with La_{CN}/Sm_{CN} of
261 0.834-1.244, La_{CN}/Yb_{CN} of 0.692-1.572 and Eu/Eu* of 0.87-1.2 (**Fig. C3**). Their primitive-
262 normalised patterns are relatively flat, but two samples have slightly negative Nb-anomalies with
263 Nb/Nb* of 0.594-1.017 (**Fig. 5**) and two other samples have negative Ti-anomalies. Their
264 weathering index ranges between 5.02-14.6 (**Fig. 6**).

Calc-silicate gneiss (unit f) (n = 5) has SiO_2 of 51.8-55.6 wt.%, TiO_2 of 0.99-1.23 wt.% and MgO of 2.47-7.19 wt.%. Trace element ranges are: 53.5-69.3 ppm Zr, 2.3-3.5 ppm Nb, 20.6-29.4 ppm Y, 44.9-156 ppm Ni and 110-254 ppm Cr. Their chondrite-normalised REE patterns are mostly flat, but slightly depleted in LREE with La_{CN}/Sm_{CN} of 0.768-1.07, La_{CN}/Yb_{CN} of 0.687-1.01 and Eu/Eu* of 0.84-1.2 (**Fig. C3**). Their primitive-normalised patterns are overall flat, but they have slightly negative Nb-anomalies with Nb/Nb* of 0.700-1.06 (**Fig. 5**). Their weathering index ranges between 9.9-18.1 (**Fig. 6**).

Garnet-rich gneiss (unit grt) (n = 4) has SiO_2 of 44.5-53.9 wt.%, TiO_2 of 1.93-2.69 wt.% and MgO of 2.44-5.79 wt.%. Trace element ranges are: 129-179 ppm Zr, 6.2-9.9 ppm Nb, 32.4-47.7 ppm Y, 18.8-137 ppm Ni and 41.1-248 ppm Cr. Their chondrite-normalised REE patterns are slightly enriched with La_{CN}/Sm_{CN} of 1.163-1.642, La_{CN}/Yb_{CN} of 0.717-2.32 and Eu/Eu* of 0.84-1.25 (**Fig. C3**). Their primitive-normalised patterns are also enriched, but they have negative Nb-anomalies with Nb/Nb* of 0.52-0.96 (**Fig. 5**). Their weathering index range between 13.6-20.9 (**Fig. 6**).

Biotite gneiss (unit b) (n = 10) has SiO_2 of 49.7-66.3 wt.%, TiO_2 of 0.54-1.44 wt.% and MgO of 2.96-6.41 wt.%. Trace element ranges are: 99.7-178 ppm Zr, 5.1-16 ppm Nb, 15.8-29.4 ppm Y, 65.9-259 ppm Ni and 113-636 ppm Cr. Their chondrite-normalised REE patterns are enriched with La_{CN}/Sm_{CN} of 2.70-4.51, La_{CN}/Yb_{CN} of 5.28-10.6 and Eu/Eu* of 0.58-0.85. Their primitive-normalised patterns are enriched, but they have negative Nb-anomalies with Nb/Nb* of 0.16-0.37 (**Fig. 5**). Their weathering index ranges between 19.0-51.8 (**Fig. 6**).

Quartzite (unit q) (n = 3) has SiO_2 of 82.1-95.1 wt.%, TiO_2 of 0.18-0.47 wt.% and MgO of 0.08-1.19 wt.%. Trace element ranges are: 59.3-154 ppm Zr, 2.2-4.0 ppm Nb, 3.0-10 ppm Y, 0.91-75 ppm Ni and 103-331 ppm Cr. Their chondrite-normalised REE patterns are highly enriched with La_{CN}/Sm_{CN} of 3.58-4.47, La_{CN}/Yb_{CN} of 17.0-33.7 and Eu/Eu* of 0.36-0.86 (**Fig. C3**). Their

primitive-normalised patterns are also highly enriched and they have large negative Nb-anomalies with Nb/Nb* of 0.099-0.232 (**Fig. 5**). Their weathering index ranges between 30.1-93.1 (**Fig. 6**).

Below we briefly summaries the main geochemical features of the few rocks that we have analysed from the Storø Anorthosite Complex. However, we must emphasise that the topic of this study is mainly the SSB and thus we do not present geochemical plots for the SAC, also due to the very limited data set that we have for the latter. The anorthosite (n = 1) has high Al_2O_3 of 33.84 wt.% and CaO of 15.73 wt.%, consistent with its mineralogy of almost pure plagioclase. The Cr and Ni contents is low with 13.7 and 10 ppm, respectively. It has slightly enriched REE patterns with La_{CN}/Sm_{CN} of 1.75, La_{CN}/Yb_{CN} of 2.25 and Eu/Eu* of 2.83. The gabbroic amphibolite (unit ag) (n = 1) has SiO_2 of 45.32 wt.%, TiO_2 of 0.71 wt.% and MgO of 4.01 wt.%. It has slightly enriched REE patterns with La_{CN}/Sm_{CN} of 1.46, La_{CN}/Yb_{CN} of 1.57 and Eu/Eu* of 1.66. The layered amphibolite (unit av) (n = 2) have SiO_2 of 46.81-49.52 wt.%, TiO_2 of 1.38-1.85 wt.% and MgO of 5.90-6.21 wt.%. They have flat to slightly depleted REE patterns with La_{CN}/Sm_{CN} of 0.55-0.92, La_{CN}/Yb_{CN} of 0.43-1.00 and Eu/Eu* of 1.08-1.67.

5.2. Bulk-rock Sm-Nd isotope data

Based on our new and previously published U-Pb zircon ages (**Section 5.3**; van Gool et al., 2007; Szilas and Garde, 2013), we have calculated initial εNd_t for the samples from the Storø Supracrustal Belt (SSB) at 2800 Ma and at 3050 Ma for samples from the Storø Anorthosite Complex (SAC), respectively. We have used the CHUR value of Bouvier et al. (2008) and a ^{147}Sm decay constant of 6.54×10^{-12} (Lugmair and Marti, 1978). Errors on the εNd_t are ±0.5 ε-units. We report DM model ages based on the estimate of Goldstein (1988). However we must point out that such model age calculations are highly uncertain and we do not want to put too much emphasis on

these ages, which may be geologically meaningless if the Sm-Nd systematics were disturbed during later events. The Sm-Nd isotopic data are available in the supplementary **Table 2**.

Two of the Storø amphibolite (unit a) samples (487919 and 487497) have εNd_{2800Ma} of 2.2 and 2.1, and model ages of 3277 and 3154 Ma, respectively. One other sample (487419) has εNd_{2800Ma} of 3.4 and a model age of 2888 Ma. The two garnet amphibolites of the SSB have εNd_{2800Ma} of 4.3 and 5.4 and model ages of 2658 and 2200 Ma, respectively.

The anorthosite sample (KSZ-09) has εNd_{3050Ma} of 2.5 and a model age of 3366 Ma. The ag amphibolite (KSZ-10) also has εNd_{3050Ma} of 2.5 and its model age is 3273 Ma.

Figure 7 shows the εNd_t evolution of all measured samples. Note the wide range in the initial εNd_t for the SSB samples and that two samples (487919 and 487497) appear to overlap with the tighter range seen for the SAC.

5.3. In situ zircon U-Pb isotope data

Zircon was separated from the biotite gneiss (KSZ-06) and the quartzite (KSZ-13) units of the Storø Supracrustal Belt (SSB), as well as from the gabbroic amphibolite (unit ag) (KSZ-10) from the Storø Anorthosite Complex (SAC). The U-Pb isotope data are presented in **Table 3** in the online supplementary material. All U-Pb age plots and unmixing ages were done with Isoplot (Ludwig, 2003). The zircon grains were inspected by scanning electron microscope (SEM) prior to ablation. Most grains are characterised by cores with normal magmatic oscillatory zoning and homogenous metamorphic rims, in line with the observations of van Gool et al. (2007), who presented detailed imaging of zircon from a broad range of lithological units from Storø. We measured both magmatic cores and metamorphic rims by LA-ICP-MS. Only data which are ±10% concordant are present in

the probability density diagrams (PDD). There is good agreement between Th/U ratios and the textural context of the laser spots, so that in general cores have low ratios and rims have high ratios.

In **Figure 8** the biotite gneiss (KSZ-06) and the quartzite (KSZ-13) show distinct detrital populations, as also reported by van Gool et al. (2007) for the same lithological units. The youngest peak is seen between 2600 and 2700 Ma. The biotite gneiss shows a main peak around 2800 Ma, whereas the quartzite has a wider peak centred at 2900 Ma. The biotite gneiss (unit b) has an additional, but significant peak at 2780 ±11 Ma according to a peak unmixing model by Isoplot and the quartzite has a small peak at around 3230 Ma.

The gabbroic amphibolite (unit ag) sample from the SAC has one distinct peak at ca. 3050 Ma and a smaller sub-peak between 2800-2600 Ma (**Fig. 9a**). The concordia diagram for sample KSZ-10 (**Fig. 9b**) was done with a model-2 fit in Isoplot (Ludwig, 2003) on the data, which were ±10% concordant and after the obvious metamorphic sub-peak at <2800 Ma was filtered out of the data. This yields an age of 3037 ±19 Ma (MSWD = 2.3), which is analytically identical (within error) to the ages reported from this units by Szilas and Garde (2013) and van Gool et al. (2007).

6. Discussion

6.1. Geochemical features of the Storø rocks

Archaean volcanic rocks have commonly undergone syn-volcanic alteration and could have experienced several metamorphic events, which may have mobilised some of the more mobile elements (e.g. Cann, 1970; Polat and Hofmann, 2003; Ordóñez-Calderón et al., 2011; Szilas and Garde, 2013). The Storø supracrustal rocks have indeed been affected by metamorphism (**Appendix A.1**) and some of the rock units are clearly premetamorphic alteration products (e.g. units ‘f’ and

360 'grt'; see Knudsen et al., 2007; Szilas, 2008; Szilas and Garde, 2013). Therefore, we will not
361 consider the mobile elements, such as the large ion lithophile elements (LILE, e.g. Rb, Cs, Sr, Pb)
362 and rely exclusively on the more immobile elements for the interpretation of the trace element
363 diagrams (**Fig. 5**). We apply the weathering index of Ohta and Arai (2007) in order to evaluate the
364 degree of weathering/alteration of the various aluminous schists and quartzites. It should be noted
365 that even unaltered volcanic rocks have a slightly elevated weathering index, as they will be
366 confined to the igneous evolution trend (**Fig. 6**).

367 In the following we are mainly discussing the new geochemical data and clearly state if we a
368 including the results of previous work for interpretations of the Storø rocks. The amphibolite (unit
369 a) shows essentially no variation that can be interpreted in terms of magmatic crystal fractionation,
370 but the data simply form a cloud of data when the various elements are plotted against SiO_2 or MgO
371 (**Fig. C4-C5**). This was also noted by Pedersen (1996), who suggested that the amphibolites may
372 represent a single basaltic eruption. However, it is more likely that the scatter simply reflects
373 metasomatic disturbance of some of the major elements, and in particular SiO_2 and MgO, which are
374 notoriously mobile. We do not mean to rule out the role of crystal fractionation in these rocks,
375 which is clearly present as seen from co-variations of the immobile incompatible trace elements, but
376 the disturbance of SiO_2 and MgO makes it difficult to quantify any potential crystal fractionation.

377 The amphibolites are metaluminous (**Fig. C6**) and can easily be discriminated from the alteration
378 products (units 'f' and 'grt') and the metasediments (units 'b' and 'q'), which are peraluminous.
379 This is indeed also obvious on **Figure 6**, where the former plot on the igneous trend, whereas the
380 latter plot within the weathered/altered field. Many of the garnet amphibolite samples likely
381 represent slightly altered basalts derived from the same protolith as the regular amphibolites
382 (basalts), with which they are interlayered. However, minor changes in their bulk composition, such
383 as loss of Na_2O and MgO could have led to residual increase in Al_2O_3 and thus garnet would

become stable during later amphibolite facies metamorphism. This is indicated by their slightly elevated Al/Na+K (**Fig. C6**) and their position above the igneous fractionation trend in the MFW diagram (**Fig. 6**). Nevertheless, the garnet amphibolites show the same overall geochemical characteristics as the least altered amphibolites (unit a) and we therefore consider the potential alteration to be mild.

The amphibolites generally plot with the tholeiitic field in various classification diagrams (**Figs. C7-C9**) and the protolith composition is indicated to be basaltic in plots that 'see through' element mobility, such as the Nb/Y-Zr/Ti diagram of Pearce (1996) (**Fig. C10**). Immobile high field strength elements (HFSE), such as Hf, Zr and Nb are useful monitors of geotectonic affinity for volcanic rocks in combination with their primitive mantle-normalised trace element signatures. Tectonic discrimination plots (see references in Rollinson, 1993) may serve as a first order guide for interpreting the original environment of allochthonous volcanic rocks. The least altered amphibolites (unit a) plot intermediate between the fields of mid-ocean ridge basalts (MORB) and island arc tholeiites (IAT) in such diagrams (**Figs. C11-C14**), and thus suggest a possible subduction zone affinity, as also argued by Ordóñez-Calderón et al. (2011). This is also observed for many other mafic supracrustal belts in southern West Greenland (e.g. Szilas et al., 2012a, 2012b, 2013a, 2013b). Despite the limitations of such discrimination diagrams the primitive mantle-normalised trace element pattern of the amphibolites (**Fig. 5**), also suggests an arc affinity for these mafic rocks. This is evident from the distinct negative Nb-anomalies (Nb/Nb* = 0.30-0.90) and elevated Th contents relative to what would be expected for MORB. Because it is difficult to achieve a negative anomaly in mafic rocks by crustal contamination, Nb anomalies are usually explained by fractionation of phases such as rutile, ilmenite or cpx in the generation of hydrous arc-related magmas (Brenan et al., 1994; Baier et al., 2008). However, negative HFSE-anomalies could equally well be explained by melting of a previously depleted mantle source, which was re-enriched

by fluid-mobile elements, which would also be compatible with fluid fluxed melting in an arc setting (Ryerson and Watson, 1987).

Additionally, the amphibolites plot above the mantle array and within the field of arc-related magmas in Th/Yb vs. Nb/Yb as defined by Pearce (2008) (**Fig. 10**). Although some of this trend could be due to small degrees of crustal contamination, as is suggested from the Sm-Nd systematics (**Section 6.2**), much of the variation occurs parallel to the mantle array and thus cannot be entirely due to magma contamination (AFC-processes). This trend is likely caused by Th-enrichment in their mantle source region, because Th can be contributed by supercritical fluids or small degree melts, which is commonly observed in subduction zone magmas (Kessel et al., 2005). Overall the geochemical features of the amphibolites in the SSB point towards an arc-related setting, but they could be compatible with either a forearc or backarc setting due to their transitional MORB and IAT features. Indeed, an environment has previously been proposed for the SSB (e.g. Polat, 2005; Knudsen et al., 2007; van Gool et al., 2007; Szilas, 2008; Ordóñez-Calderón et al., 2011).

The garnet-rich gneiss (unit grt) was originally mapped as part of the biotite gneiss (unit b) and from its mineral assemblage it was interpreted as being a metasedimentary rock (Grahl-Madsen, 1994; Skyseth, 1997; Smith, 1998; Polat, 2005; Persson, 2007). However, it was noted that the geochemical compositions of these rocks are peculiar and dissimilar to other Archaean metasedimentary lithologies (cf. Taylor and McLennan, 1985). The garnet-rich gneisses are peraluminous and have Al_2O_3 up to 21 wt.% (due to loss of CaO and MgO), which resulted in abundant sillimanite and garnet during metamorphism. Field relationships show enclaves of unaltered amphibolite with gradational contacts present within the garnet-rich gneiss (unit grt), which together with their geochemical features, are now generally accepted as evidence of this unit being an alteration product of the basaltic protolith of the amphibolite (unit a) (van Gool et al., 2007; Knudsen et al., 2007; Szilas, 2008; Szilas and Garde, 2013). The ratios of immobile elements

are overlapping with those of the amphibolite (unit a), supporting their common origin. Residual enrichment of immobile trace elements, combined with addition of LREE during premetamorphic seafloor weathering is thought to be the cause of the unusual composition of the garnet-rich gneisses (Szilas and Garde, 2013). Gold and sulfide occurs along this lithological contact, as well as within the amphibolite (unit a) (Østergaard and van Gool, 2007). However, Szilas and Garde (2013) concluded that the Au mineralisation and the aluminous alteration documented in the garnet-rich gneiss (unit grt) are unrelated.

The calc-silicate gneiss (unit f), found as schlieren within the amphibolite, has also been suggested to be an alteration product of the amphibolite (unit a) (van Gool et al., 2007; Szilas, 2008). This is supported by the fact that the two rock types have the same ratios of immobile elements, but with slightly lower abundances in the calc-silicate gneiss, indicating dilution of the trace elements by a net mass addition during alteration. This can perhaps be explained by veining or pervasive alteration that added components. The calc-silicate gneiss is aluminous with an average Al_2O_3 content of around 17 wt.%. This is seen in the mineralogy as abundant garnet and plagioclase. SiO_2 and K_2O are slightly elevated compared to the amphibolites, but MgO and CaO are generally lower (**Fig. C4**). The REE pattern is flat for the HREE, but a small positive inclination is present for the LREE, suggesting that they were enriched during the alteration (**Fig. C3**). Based on the above it is unlikely that the calc-silicate gneiss represents a sedimentary rock. Attempts to extract zircon from this rock have been unsuccessful and thus an origin by premetamorphic alteration of basalt, which also does not contain zircon, is compatible with all observations, as also suggested by previous work (van Gool et al., 2007; Szilas, 2008).

The biotite gneiss (unit b) and the quartzite (unit q) both have relatively high weathering indices (19.0-51.8 and 30.1-93.1, respectively) (**Fig. 6**), as would be expected for a sedimentary protolith. A sedimentary origin is thus likely from the overall mineralogy (quartz, biotite and garnet) and the

456 detrital U-Pb age populations of zircon supports this interpretation (see **Section 5.3** and **Appendix**
457 **A.2**; van Gool et al., 2007; Scherstén et al., 2012). The modal and geochemical variations of this
458 rock suggest an origin as immature volcanogenic sediment (Pedersen, 1996; van Gool et al., 2007).
459 Their primitive mantle-normalised trace element patterns suggest that both the biotite gneiss (unit b)
460 and the quartzite (unit q) have contributions from incompatible trace element rich components,
461 which was likely derived from an evolved source similar to the regional TTG gneisses (**Fig. 5**). This
462 is also corroborated by their U-Pb zircon age distribution, which shows many well-known age
463 peaks from the surrounding orthogneiss terranes (Nutman et al., 2007; van Gool et al., 2007). The
464 HREE and HFSE part of their trace element patterns indicates that the biotite gneisses additionally
465 contain a significant mafic component. In contrast the quartzites must mainly have been derived by
466 weathering of TTG gneisses, as seen by their highly incompatible trace element enriched patterns
467 (**Fig. 5**) and their position relative to the MF-igneous trend in **Figure 6**. However, the presence of
468 abundant fuchsite in the quartzites suggests that they also have contributions from Cr-rich sources.
469 This could be represented by chromitite-bearing ultramafic enclaves, which are found scattered
470 throughout the Itsaq gneisses (e.g. Bennett et al., 2002).

471 An alternative model of hydrothermal alteration of TTG-type orthogneisses to form the
472 quartzites could be envisioned, and we have tested this possibility by making mass-balance
473 calculations using the isocon method (Grant, 1986, 2005) and assumed that TiO_2, Zr and Lu would
474 remain immobile. We used the median composition of the Itsaq TTG-orthogneisses published by
475 Hoffmann et al. (2014) as a potential precursor rock and tested what changes would be required to
476 convert this to the compositions of our three quartzite samples (**Figs. C15-17**). The results show
477 that there would be required significant external addition of Cr, V and Co, but loss of Al. Given that
478 these elements are generally considered to be immobile during hydrothermal alteration (Polat and
479 Hofmann, 2003; Szilas and Garde, 2013) it appears unlikely that alteration of TTG gneisses could

be responsible for the formation of the quartzite (unit q). This is indeed supported by the detrital zircon population found in these rocks (**Section 5.3**; van Gool et al., 2007). It seems more likely that the compatible elements represent sedimentary accumulation of chromite, which is abundant in the ultramafic enclaves found in the regional TTG gneisses.

Although we only have preliminary data from the Storø Anorthosite Complex (SAC) we would like to point out a few geochemical features of these rocks. Firstly, the anorthosite has very distinct positive Pb, Sr and Eu anomalies, which are also known from similar rocks in the Fiskenæsset region (Polat et al., 2011b). Interestingly, a corresponding depletion is not seen in the assumed co-genetic 'av' and 'ag' amphibolites. While the 'av' amphibolites resemble the amphibolites of the SSB in terms of trace element patterns and abundances, the 'ag' amphibolite has low trace element abundances (close to PM values). The 'ag' amphibolite further has the same positive Pb, Sr and Eu anomalies as the anorthosite in addition to a large positive Ti-anomaly. The observation that 'ag' amphibiolites are included/intruded in the 'av' amphibolites suggests that the latter may represent the basement, which the SAC intruded. Unfortunately, we do not have isotope data to support this claim and future studies will have to establish the temporal differences in detail.

6.2. Bulk-rock Sm-Nd isotope systematics

The low ∑REE of the anorthosite sample (KSZ-09) leaves it prone to late metamorphic disturbance, although the initial εNd_{3050Ma} of 2.5 is in good agreement with a DM source at 3050 Ma. The 'ag amphibolite' (KSZ-10) also has low ∑REE (close to the primitive mantle value) and is thus also susceptible to metamorphic overprinting. However, this sample also has initial εNd_{3050Ma} of 2.5, which is consistent with a DM source. Archaean gabbro-anorthosite complexes in SW Greenland are generally believed to have formed in oceanic arc-related settings (e.g. Hoffmann et

al., 2011b; Polat et al., 2011b; Huang et al., 2012), and this is in good agreement with the generally juvenile composition of these two samples from the Storø Anorthosite Complex (SAC). Thus, the geochemistry and the Sm-Nd isotope compositions suggest that the SAC could have formed in a juvenile island arc at around 3050 Ma, as indicated by the new U-Pb zircon age of sample KSZ-10. These zircon grains generally have low Th/U ratios consistent with magmatic origins.

The two garnet amphibolite samples (487907 and 489709) from the Storø Supracrustal Belt (SSB), which have likely experienced some degree of alteration, as seen by their elevated Al_2O_3/K_2O+Na_2O ratio (**Fig. C6**), have the highest initial εNd_{2800Ma} (4.3 and 5.4) of all measured samples. Alteration or possible contamination is also suggested from the co-variation of Nb/Nb* and Th/Yb vs. εNd_t (**Fig. 11**). However, the high initial εNd_{2800Ma} cannot be explained by crustal contamination, because they plot above the DM trend, whereas continental crust would be expected to have negative values at 2800 Ma. Early alteration would also not be expected to change the initial Nd-isotope compositions, unless radiogenic Nd was introduced with such fluids. Although we noted above that the Sm-Nd systematics of the SAC samples with low ∑REE do not appear to have been disturbed, it is possible that the presence of garnet have resulted in different partition behaviour. Thus, given the elevated Nd-compositions in the garnet amphibolites it seems more likely that disturbance of the Sm-Nd systematics occurred during late (2630 Ma) metamorphism when garnet had formed, which for some reason affected these garnet-bearing samples more severely than the garnet-free samples. Alternatively, these high initial εNd_{2800Ma} values could be an artefact of incomplete digestion of refractory garnet prior to isotope analysis. Clearly, more isotope data is needed for the SSB to resolve such issues.

The main amphibolites (unit a) show model ages that are older than their proposed age of <2800 Ma (c.f. van Gool et al., 2007). Their εNd_{2800Ma} ranges from 2.2-3.4 and thus one sample (487919) plots right on the DM trend (**Fig. 7**), whereas the two others plot slightly below. The two latter

528 samples may contain a small contribution from continental crust-derived sediments, as indicated by
529 their lower MgO relative to sample 487919. This would be a reasonable interpretation, given the
530 close proximity to the thick, mature sedimentary package represented by the biotite gneiss (unit b)
531 and quartzite (unit q). However, this felsic component could either represent sediments from older
532 continental crust or it could simply reflect a contribution from felsic melts derived from a
533 subducting slab in an arc setting.

534 In order to test if the contamination that is suggested from the isotope data is supported by the
535 trace element compositions of these rocks, we have carried out assimilation-fractional-
536 crystallisation (AFC) modelling (DePaolo, 1981). We have tested several possible contaminants:
537 the estimate for the continental crust of Rudnick and Gao (2003), local TTG orthogneiss (Hoffmann
538 et al., 2014) and Storø metasediments (this study). We find that the trace element patterns (**Fig. 5**)
539 and the displacement above the mantle array in the Pearce-diagram (**Fig. 10**), can indeed be
540 accounted for by assimilation of the most primitive Storø amphibolite by continental crust in
541 combination with less than 10% crystal fractionation (50% olivine, 30% plagioclase and 20% cpx)
542 at a reasonable r-value of 0.3 (**Figs. C18 and C19**). Therefore, the incompatible trace elements and
543 the Nd-isotope compositions of the Storø rocks are consistent with minor contamination. Pure AFC-
544 processes involving regional TTG gneiss or Storø metasediments are not a good fit with the data
545 (**Figs. C20-25**), whereas continental crust (Rudnick and Gao, 2003) could have been viable
546 contaminant, because it would only require very small degrees of assimilation. However, the AFC-
547 model is only capable of explaining the displacement above the mantle array (**Fig. 10, C18**) and not
548 the internal variation. Mantle overprinting with either slab-derived felsic melts or partial melts from
549 subducted sediments could also explain the observed displacement. With the limited number of
550 samples in our current isotope data set we cannot distinguish between these two alternatives with
551 confidence. However given the widespread presence of regional Eoarchaean crust and the lack of

552 xenocrystic zircon in the mafic samples, despite multiple attempts to separate zircon, we tend to
553 lean towards a model, which invokes a slab derived contribution (ca. 10%) followed by minor
554 fractional crystallisation of the mafic magma. This also fits better with the AFC-modelling (**Figs.**
555 **C18-25**). This would imply a subduction model with partial melting of MORB of a similar age as
556 the SAC and could account for the fact that two of the amphibolites from the SSB appear to have
557 interacted with the SAC (**Fig. 7**). Alternatively, SAC represents the basement through which the
558 volcanism associated with the SSB erupted and deposited onto. Future isotope studies (preferably
559 using the immoble Lu-Hf system) are needed to establish the total range of isotopic variation of the
560 SSB and SAC, because the Sm-Nd system is susceptible to metamorphic disturbance and thus these
561 results are not unequivocal. Furthermore, it is recommended that also the 'ag' amphibolites are
562 measured to establish if they are part of the SSB or SAC or if they in fact represent the basement,
563 which the anorthosite complex intruded.
564
565 6.3. U-Pb zircon age constraints
566
567 Our U-Pb zircon data confirm the previous interpretation that the SSB has an age of <2800Ma,
568 whereas the SAC has an age of ca. 3050 Ma (van Gool et al., 2007; Szilas and Garde, 2013).
569 However, our data hints at an even younger minimum age of 2780 ±11 Ma from the small detrital
570 population observed in the biotite gneiss (KSZ-06) as seen in **Figure 8a**. Nevertheless, because this
571 peak could have been affected by Archaean lead loss and displaced along the concordia we do want
572 to over-interpret the significance of this small peak. On the over hand the 3050 Ma age seems to be
573 a fairly robust estimate for the SAC, given that several studies have now arrived at this age (Hollis,
574 2005; van Gool et al., 2007; Szilas and Garde, 2013).
575

576 6.4. A new geodynamic model for the Storø Supracrustal Belt

577

578 As discussed above (**Section 6.2**), we suggest that the Storø Anorthosite Complex (SAC) formed
579 in a juvenile island arc complex at ca. 3050 Ma, consistent with the Sm-Nd isotope data and the
580 anorthosite model of Hoffmann et al. (2011b). From our geochemical data the <2800 Ma Storø
581 Supracrustal Belt (SSB) represents arc-related oceanic crust formed either in a forearc or backarc
582 setting, as also suggested by previous geochemical studies (van Gool et al., 2007; Ordóñez-
583 Calderón et al., 2011).

584 The question remains whether the SAC represents the basement onto which the SSB was
585 deposited and thus contamination of the SSB magmas happened in situ, or alternatively the
586 supracrustal rocks accreted to the SAC during local terrane amalgamation (2720-2635 Ma) and was
587 simply contaminated by a slab-derived component of similar age as the SAC. With the currently
588 available data we cannot distinguish between these two models. Nevertheless, the mafic crust of the
589 SSB apparently formed a basin in proximity to uplifted continental crust, which contributed with
590 significant volumes of mature clastic sediments (now quartzites) that also mixed locally with
591 material derived from mafic to ultramafic sources (now biotite gneisses).

592 The high maturity of the quartzites (SiO_2 > 82 wt.%; W-index of 30-90), as well as their
593 abundance (**Fig. C2**), is an important constraint on the geodynamic setting of the SSB. This was
594 perhaps underestimated by Ordóñez-Calderón et al. (2011), who concluded that the Storø
595 supracrustal rocks formed in a distal island arc setting. However, the general scarcity of clastic
596 sediments within Archaean supracrustal belts in southern West Greenland testifies to limited
597 continental freeboard during their time of formation. This is consistent with the global evidence for
598 lack of significant topographic relief during the Archaean and the observation that Archaean
599 supracrustal belts are mostly comprised of subaqueous volcanic rocks, both of which are thought to

600 be a consequence of a hotter and thus weaker mantle and lower crust during the Archaean (Flament
601 et al., 2008, 2011). Additionally, the calculations of Pope et al. (2012) showed that the ocean
602 volume was likely significantly larger (ca. 25% relative to present) during the Archaean and thus
603 subaerial continent exposures would have been rare. In this light it is remarkable to find highly
604 mature sediments in the SSB, in great abundances and with local provenance. This clearly suggests
605 that the <2800 Ma SSB represents arc-related oceanic crust that formed in a proximal setting with
606 subaerially exposed continental crust available to supply sediment and therefore likely represents a
607 back-arc basin. Furthermore, the presence of mature continent-derived sediments implies that the
608 temperature of the mantle and lower crust in this region was low enough to support a large orogen
609 ca. 2800 Ma when these sediments were deposited. Another example of evidence for subaerial
610 continent exposure was recently presented by Viehmann et al. (2013) for Neoarchaean rocks from
611 Canada. They found that significant amounts of radiogenic Hf was present in BIFs and this could
612 only be explained by erosion of continental crust. Thus, there is some evidence for the subaerial
613 emergence of continents in at least some parts of the world during this period of Earth's history.
614 The SAC and the SSB were amalgamated between the Akia terrane to the west and the Itsaq
615 gneiss complex to the east from around 2720 Ma and no later than 2630 Ma, which represents the
616 latest peak metamorphic event in these rocks (Hollis, 2005). Our proposed model of differential
617 evolution of the SSB and the SAC is compatible with the long held notion that the Nuuk region
618 formed through the accretion of discrete volcanic arcs and thus represents an analogue to modern-
619 type orogenic systems (Nutman et al., 1989; Friend and Nutman, 1991; McGregor et al., 1991;
620 Windley and Garde, 2009). The final suturing stage of this accretionary assemblage is represented
621 by the post-tectonic Qôrqut granite, which intruded during a period of thermal relaxation at about
622 2550 Ma (Nutman et al., 2010).
623

7. Conclusions

The geochemical data presented in this paper from the island of Storø are broadly compatible with a subduction zone setting, as also suggested by previous work (e.g. Ordóñez-Calderón et al., 2011; van Gool et al., 2007). We have established the formal names the 'Storø Supracrustal Belt' (SSB) for the <2800 Ma supracrustal sequence and the 'Storø Anorthosite Complex' (SAC) for the ca. 3050 Ma gabbro-anorthosite sequence, which crop out on in the central part of Storø.

Our new Sm-Nd isotope data indicates that the ca. 3050 Ma SAC likely represents remnants of a juvenile island arc. From this isotope data we can rule out the possibility of significantly old crustal contamination of the SSB, but we cannot determine whether these rocks extruded through and deposited onto the SAC, or if the mantle source of the SSB was simply contaminated by a slab or sediement melt component of similar age as the SAC.

The SSB contains large volumes of mature clastic sedimentary rocks with a detrital zircon age populations derived from regionally well-known orthogneiss terranes. This suggests formation in a continent proximal environment, such as backarc basin, and that there was considerable topography and freeboard in order to produce these mature sediments. The latter suggests that large orogens had formed at least locally by 2800 Ma when these sediments were deposited. Collectively, the data presented in this paper supports the occurrence of modern-style subduction zone environments during the Meso- to Neoarchaean.

Acknowledgements

We acknowledge the Greenland Bureau of Minerals and Petroleum (BMP) and the Geological Survey of Denmark and Greenland (GEUS) for financial support of the field and analytical work. Much of the field work that forms the basis for this paper was carried out in cooperation with, and

co-financed by NunaMinerals A/S. We thank Agnete Steenfelt for comments on an early version of the manuscript and acknowledge Claus Østergaard and Adam A. Garde for many fruitful discussions about the Storø rocks over the years. We also thank Fiorella Fabra Aguilera and Mojagan Alaei for help with zircon separation at GEUS. The incisive comments of two anonymous reviewers significantly improved the manuscript. We thank Guochun Zhao for the editorial handling of the manuscript. A. Scherstén acknowledges financial support from the Swedish Research council through grant #2008-3447. K. Szilas was supported by grant #12-125873 from the Danish Council for Independent Research. This study is a contribution to IGCP project 599.

References

Baier, J., Audétata, A., Keppler, H., 2008. The origin of the negative niobium tantalum anomaly in subduction zone magmas. Earth and Planetary Science Letters 267, 290-300.

Bédard, J.H., 2006. A catalytic delamination-driven model for coupled genesis of Archaean crust and sub-continental lithospheric mantle. Geochimica et Cosmochimica Acta 70, 1188-1214.

Bennett, V.C., Nutman, A.P., Esat, T.M., 2002. Constraints on mantle evolution from $^{187}Os/^{188}Os$ isotopic compositions of Archean ultramafic rocks from southern West Greenland (3.8 Ga) and Western Australia (3.46 Ga). Geochimica et Cosmochimica Acta 66, 2615-2630.

Bouvier A., Vervoort J.D., Patchett P.J., 2008. The Lu–Hf and Sm–Nd isotopic composition of CHUR: Constraints from unequilibrated chondrites and implications for the bulk composition of terrestrial planets. Earth and Planetary Science Letters 273, 48-57.

Brenan, J.M., Shaw H.F., Phinney D.L., Ryerson, F.J., 1994. Rutile-aqueous fluid partitioning of Nb, Ta, Hf, Zr, U, and Th: implications for high field strength element depletions in island-arc basalts. Earth and Planetary Science Letters 128, 327-339

Bridgewater, D., Schiøtte, L., 1991. The Archaean gneiss craton of northern Labrador. A review of current results, ideas and problems. Bulletin of the Geological Society of Denmark 39, 133-153.

Cann, J.R., 1970. Ocean floor basaltic rocks. Earth and Planetary Science Letters 10, 7-11.

679 Crowley, J.L., 2003. U–Pb geochronology of 3810–3630 Ma granitoid rocks south of the Isua greenstone belt, southern West Greenland. Precambrian
680 Research 126, 235-257.
681
682 Davies, G.F., 1999. Dynamic Earth Plates, Plumes and Mantle Convection. Cambridge University Press, 458 pp.
683
684 DePaolo, D.J., 1981. Trace element and isotopic effects of combined wallrock assimilation and fractional crystallization. Earth and Planetary Science
685 Letters 53, 189-202.
686
687 Dilek, Y., Polat, A., 2008. Suprasubduction zone ophiolites and Archaean tectonics. Geology 36, 431-432.
688
689 Dziggel, A., Diener, J.F.A., Kolb, J., Kokfelt, T.F., 2014. Metamorphic record of accretionary processes during the Neoarchaean: The Nuuk region,
690 southern West Greenland. Precambrian Research 242, 22-38.
691
692 Flament, N., Coltice, N., Rey, P.F., 2008. A case for late-Archaean continental emergence from thermal evolution models and hypsometry. Earth and
693 Planetary Science Letters 275, 326-336.
694
695 Flament, N., Rey, P.F., Coltice, N., Dromart, G., Olivier, N., 2011. Lower crustal flow kept Archean continental flood basalts at sea level. Geology
696 39, 1159-1162.
697
698 Friend, C.R.L., Nutman, A.P., 1991. Refolded nappes formed during late Archaean terrane assembly, Godthåbsfjord, southern West Greenland.
699 Journal Geological Society of London 148, 507-519.
700
701 Friend, C.R.L., Nutman, A.P., 2005. New pieces to the Achaean terrane jigsaw puzzle in the Nuuk region, southern West Greenland: steps in
702 transforming a simple insight into a complex regional tectonothermal model. Journal of the Geological Society of London 162, 147-162.
703
704 Friend, C.R.L., Nutman, A.P., 2010. Eoarchean ophiolites? New evidence for the debate on the Isua supracrustal belt, southern West Greenland.
705 American Journal of Science 310, 826–861.
706
707 Friend, C.R.L., Nutman, A.P., McGregor, V.R., 1987. Late-Archaean tectonics in the Færingehavn-Tre Brødre area, south of Buksefjorden, southern
708 West Greenland. Journal of the Geological Society of London 144, 369-376.
709
710 Friend, C.R.L., Nutman, A.P., McGregor, V.R., 1988. Late Archaean terrane accretion in the Godthåb region, southern West Greenland. Nature 335,
711 535-538.
712
713 Friend, C.R.L., Nutman, A.P., Baadsgaard, H., Kinny, P.D., McGregor, V.R., 1996. Timing of late Archaean terrane assembly, crustal thickening and
714 granite emplacement in the Nuuk region, southern West Greenland. Earth and Planetary Science Letters 142, 353-365.

Furnes, H., Dilek, Y., de Wit, M., 2013. Precambrian greenstone sequences represent different ophiolite types. Gondwana Research (in press).

Furnes, H., de Wit, M., Dilek, Y., 2014. Precambrian Greenstone Belts Host Different Ophiolite Types. In: Evolution of Archean Crust and Early Life, pp. 1-22. Springer Netherlands.

Goldstein, S.L., 1988. Decoupled evolution of Nd and Sr isotopes in the continental crust and the mantle. Nature 336, 733-738.

Grahl-Madsen, L. 1994. Storø gold project, Southwest Greenland 1994. Internal report, Nunaoil A/S. Report file 21413, 22 pp.

Grant, J.A., 1986. The isocon diagram – a simple solution to Gresens' equation for metasomatic alteration. Economic Geology 81, 1976-1982.

Grant, J.A., 2005. Isocon analysis: a brief review of the method and applications. Physics and Chemistry of the Earth 30, 997-1004.

Hamilton, W.B., 1998. Archean magmatism and deformation were not products of plate tectonics. Precambrian Research 91, 143-179.

Hamilton, W.B., 2011. Plate tectonics began in Neoproterozoic time, and plumes from deep mantle have never operated. Lithos 123, 1-20.

Hoffmann, J.E., Münker, C., Polat, A., Rosing, M.T., Schulz, T., 2011a. The origin of decoupled Hf-Nd isotope compositions in Eoarchean rocks from southern West Greenland. Geochimica et Cosmochimica Acta 75, 6610–6628.

Hoffmann, J., Svahnberg, H., Piazolo, S., Scherstén, A., Münker, C., 2011b. The geodynamic evolution of Mesoarchean anorthosite complexes inferred from the Naajat Kuuat Complex, southern West Greenland. Precambrian Research 196-197, 149-170.

Hoffmann, J., Nagel, T.J., Münker, C., Næraa, T., Rosing, M.T., 2014. Constraining the process of Eoarchean TTG formation in the Itsaq Gneiss Complex, southern West Greenland. Earth and Planetary Science Letters, 388, 374-386.

Hollis J.A. (Ed.), 2005. Greenstone belts in the central Godthåbsfjord region, southern West Greenland: geochemistry, geochronology and petrography arising from 2004 field work, and digital map data. Danmarks og Grønlands Geologiske Undersøgelse Rapport 2005/42, 215 pp.

Hollis, J.A., van Gool, J.A.M., Steenfelt, A., Garde, A.A., 2004. Greenstone belts in the central Godthåbsfjord regioin, southern West Greenland. Danmarks og Grønlands Geologiske Undersøgelse Rapport 2004/110, 110 pp.

Hollis, J.A., Frei, D., van Gool, J.A.M., Garde, A.A., Persson, M., 2006. Using zircon geochronologoly to resolve the Archaean geology of the southern West Greenland. Review of Survey activities 2005. Geological Survey of Denmark and Greenland Bulletin 10, 49-52.

751 Huang, H., Polat, A., Fryer, B. J., Appel, P. W., Windley, B. F., 2012. Geochemistry of the Mesoarchean Fiskenæsset Complex at Majorqap qâva,
752 SW Greenland: Evidence for two different magma compositions. Chemical Geology, 314, 66-82.
753
754 Kalsbeek, F., Taylor, P.N., 1983. Anatectic origin of mid-Proterozoic granite dykes in the Isukasia area, West Greenland: Pb-Pb and Rb-Sr isotope
755 evidence. Grønlands Geologiske Undersøgelse Rapport 115, 38-42.
756
757
758 Kessel, R., Schmidt, M.W., Ilmer, P., Pettke, T., 2005. Trace element signature of subduction-zone fluids, melts and supercritical liquids at 120–180
759 km depth. Nature 437, 724-727 .
760
761 Knudsen, C., van Gool, J.A.M., Østergaard, C., Hollis, J.A., Rink-Jørgensen, M., Persson, M., Szilas, K., 2007. Gold-hosting supracrustal rocks on
762 Storø, southern West Greenland: lithologies and geological environment. Geological Survey of Denmark and Greenland Bulletin 13, 41-44.
763
764 Kokfelt, T.F. (Ed.), 2011. Geochemistry of Supracrustal Rocks and Associated Intrusive TTG Suites of the Archaean Craton in South-West Greenland
765 and Southern West Greenland, 61◦30–64◦N. Geological Survey of Denmark and Greenland Report 2011/10.
766
767 Kolb, J., Dziggel, A., Schlatter, D. M., 2013. Gold Occurrences of the Archean North Atlantic Craton, southwestern Greenland: A Comprehensive
768 Genetic Model. Ore Geology Reviews 54, 29-58.
769
770 Ludwig, K.R., 2003. Isoplot/Ex 3.00. A geochronological toolkit for Microsoft Excel. Special Publication 4. Berkeley Geochronological Center,
771 Berkeley, CA.
772
773 Lugmair G.W., Marti K., 1978. Lunar initial 143Nd/144Nd: differential evolution of the lunar crust and mantle. Earth and Planetary Science Letters
774 39, 349-357.
775
776 McCall, G.J.H., 2003. A critique of the analogy between Archaean and Phanerozoic tectonics based on regional mapping of the Mesozoic-Cenozoic
777 plate convergent zone in the Makran, Iran. Precambrian Research 127, 5-17.
778
779 McGregor, V.R. (compiler), 1984. Geological map of Greenland 1:100,000 Qôrqut 64 V.1 Syd. Geological Survey of Greenland.
780
781 McGregor, V.R., Friend, C.R.L., Nutman, A.P. 1991. The late Archaean mobile belt through Godthåbsfjord, southern West Greenland: a continent-
782 continent collision zone? Bulletin of the Geological Society of Denmark 39, 179-197.
783
784 Nutman, A.P., Friend, C.R.L., 2007. Adjacent terranes with ca. 2715 and 2650 Ma high-pressure metamorphic assemblages in the Nuuk region of the
785 North Atlantic Craton, southern West Greenland: Complexities of Neoarchaean collisional orogeny. Precambrian Research 155, 159-203.

Nutman, A.P., Friend, C.R.L., Baadsgaard, H., McGregor, V.R., 1989. Evolution and assembly of Archaean gneiss terranes in the Godthåbsfjord region, southern West Greenland: structural, metamorphic, and isotopic evidence. Tectonics 8, 573-589.

Nutman, A.P., Friend, C.R.L., Barker, S.S., McGregor, V.R., 2004. Inventory and assessment of Palaeoarchaean gneiss terrains and detrital zircons in southernWest Greenland. Precambrian Research 135, 281-314.

Nutman, A.P., Christiansen, O., Friend, C.R.L., 2007. 2635 Ma amphibolite facies gold mineralisation near a terrane boundary (suture?) on Storø, Nuuk region, southern West Greenland. Precambrian Research 159, 19-32.

Nutman, A.P., Friend, C.R.L., Hiess, J., 2010. Setting of the ~2560 Ma Qôrqut Granite Complex in the Archean crustal evolution of Southern West Greenland. American Journal of Science 310, 1081-1114.

Ohta, T., Arai, H., 2007. Statistical empirical index of chemical weathering in igneous rocks: A new tool for evaluating the degree of weathering. Chemical Geology 240, 280-297.

Ordóñez-Calderón, J.C., Polat, A., Fryer, B.J., Gagnon, J.E., 2011. Field and geochemical characteristics of Mesoarchean to Neoarchean volcanic rocks in the Storø greenstone belt, SW Greenland: Evidence for accretion of intra-oceanic volcanic arcs. Precambrian Research 184, 24-42.

Østergaard, C., van Gool, J.A.M., 2007. Assessment of the gold mineralisation on Storø, Godthåbsfjord, southern West Greenland: Mineral resource assessment of the Archaean Craton (66° to 63°30'N) SW Greenland, Contribution no. 5. Danmarks og Grønlands Geologiske Undersøgelse Rapport 2007/78, 20 pp.

Pearce, J.A., 1996. A user's guide to basalt discrimination diagrams. In: Wyman, D.A. (Ed.), Trace Element Geochemistry of Volcanic Rocks: Applications for Massive Sulphide Exploration: Geological Association of Canada, 12, pp. 79-113.

Pearce, J.A., 2008. Geochemical fingerprinting of oceanic basalts with applications to ophiolite classification and the search for Archean oceanic crust. Lithos 100, 14-48.

Pedersen, N.H., 1996. Guldmineraliseringer på Storø, Sydlige Vestgrønland. Progress report, forskeruddannelsens del A. Geologisk Institut, Århus Universitet. GEUS report file 22029, 83 pp.

Persson, M., 2007. Metamorphic and geochronological evolution of the Au-bearing rocks on central Storø, Nuuk region, West Greenland. Upublished M.sc thesis, Copenhagen University.

Polat, A., 2005. Geochemical and petrographic characteristics of the Ivisaartoq and Storø greenstone belts, southern West Greenland: Progress report. In: Hollis, J.A. (Ed.), Greenstone belts in the central Godthåbsfjord region, southern West Greenland. Danmarks og Grønlands Geologiske Undersøgelse Rapport 2005/42, 215 pp.

Polat, A., Hofmann, A.W., 2003. Alteration and geochemical patterns in the 3.7-3.8 Ga Isua greenstone belt, West Greenland. Precambrian Research 126, 197-218.

Polat, A., Hofmann, A.W., Rosing, M.T., 2002. Boninite-like volcanic rocks in the 3.7–3.8 Ga Isua greenstone belt, West Greenland: geochemical evidence for intra-oceanic subduction zone processes in the early Earth. Chemical Geology 184, 231-254.

Polat, A., Appel, P.W.U., Fryer, B.J., 2011a. An overview of the geochemistry of Eoarchean to Mesoarchean ultramafic to mafic volcanic rocks, SW Greenland: Implication for mantle depletion and petrogenetic processes at subduction zones in the early Earth. Gondwana Research 20, 255-283.

Polat, A., Fryer, B. J., Appel, P. W., Kalvig, P., Kerrich, R., Dilek, Y., Yang, Z., 2011b. Geochemistry of anorthositic differentiated sills in the Archean (~ 2970Ma) Fiskenæsset Complex, SW Greenland: Implications for parental magma compositions, geodynamic setting, and secular heat flow in arcs. Lithos 123, 50-72.

Pope, E.C., Bird, D.K., Rosing, M.T., 2012. Isotope composition and volume of Earth's early oceans. Proceedings of the National Academy of Sciences of the United States of America 109, 4371, 1-6.

Rollinson, H., 1993. Using geochemical data: evaluation, presentation, interpretation. Prentice Hall, 352 pp.

Rudnick, R.L., Gao, S., 2003. Composition of the continental crust. In Holland, H.D. and Turekian, K.K. (Eds.): Treatise on Geochemistry Vol. 3, 1-64.

Ryerson, F.J., Watson, E.B., 1987. Rutile saturation in magmas: implications for Ti–Nb–Ta depletion in island-arc basalts. Earth and Planetary Science Letters 86, 225-239.

Scherstén, A., Szilas, K., Creaser, R.A., van Gool, J.A.M., Næraa, T., Østergaard, C., 2012. Re-Os and U-Pb constraints on gold mineralisation events in the Meso- to Neoarchaean Storø greenstone belt, Storø, southern West Greenland. Precambrian Research, 200-203, 149-162.

Skyseth, T., 1997. Gold exploration on Storø 1996, South West Greenland, Exploration License 13/97 (former 02/92). Internal report, Nunaoil A/S. GEUS Report file 21601, 14 pp.

Smith, G.M., 1998. Report on the structure and geometry of the gold mineralisation at Qingaq Storø, Nuukfjord, South West Greenland. Internal report, Nunaoil A/S. GEUS report file 21602, 13 pp.

Stendal, H. (Ed.), 2007. Characterisation of selected geological environments. Mineral resource assessment of the Archaean Craton (66º to 63º 30'N) SW Greenland. Contribution no. 1. Danmarks og Grønlands Geologiske Undersøgelse Rapport 2007/20, 90 pp.

Stern, R.J., 2005. Evidence from ophiolites, blueschists, and ultrahigh-pressure metamorphic terranes that the modern episode of subduction tectonics began in Neoproterozoic time. Geology 33, 557-560.

Stern, R.J., 2008. Modern-style plate tectonics began in Neoproterozoics time: an alternative interpretation of Earth's tectonic history. In: Condie, K.C., Pease, V. (Eds.),When did Plate Tectonics Begin on Planet Earth? Geological Society of America, Special Publications 440, pp. 265-280.

Sun, S., McDonough, W.F., 1989. Chemical and isotopic systematics of oceanic basalts: implications for mantle composition and processes. In: Saunders, A.D., Norry, M.J. (Eds.), Magmatism in the Ocean Basins. Geological Society of London, Special Publications 42, 313-345.

Szilas, K., 2008. Geochemistry of the late Archaean Storø supracrustal sequence and alteration zones associated with gold mineralisation, Nuuk region, southern west Greenland. Unpublished M.Sc. thesis, University of Copenhagen, 42 pp.

Szilas, K., Hoffmann, J.E., Scherstén, A., Rosing, M.T., Kokfelt, T.F., Windley, B.F., van Hinsberg, V.J., Næraa, T., Keulen, N., Frei, R., Münker, C., 2012a. Complex calc-alkaline volcanism recorded in Mesoarchaean supracrustal belts north of Frederikshåb Isblink, southern West Greenland: implications for subduction zone processes in the early Earth. Precambrian Research 208-211, 90-123.

Szilas, K., Scherstén, A., Næraa, T., Stendal, H., Rosing, M.T., Kokfelt, T.F., V.J., Frei, R., 2012b. Origin of Mesoarchaean arc related rocks with boninite/komatiite affinities from southern West Greenland. Lithos 144-145, 24-39.

Szilas, K., van Hinsberg, J., Kisters, A.F.M., J. Hoffmann, E., Kokfelt, T.F., Scherstén, A., Windley, B.F., Münker, C., 2013a. Remnants of arc-related Mesoarchaean oceanic crust in the Tartoq Group, SW Greenland. Gondwana Research 23, 436-451.

Szilas, K., Hoffmann, J.E., Scherstén, A., Kokfelt, T.F, Münker, C., 2013b. Archaean andesite petrogenesis: insights from the Grædefjord supracrustal belt, SW Greenland. Precambrian Research 236, 1-15.

Szilas, K., Garde, A.A., 2013. Mesoarchaean aluminous rocks at Storø, southern West Greenland: new age data and evidence of premetamorphic seafloor weathering of basalts. Chemical Geology 354, 124-138.

Taylor, S.R., McLennan, V.R., 1985. The Continental Crust: its Composition and Evolution. Blackwell Scientific Publications, 312 pp.

van Gool, J.A.M., Scherstén, A., Østergaard, C., Næraa, T., 2007. Geological setting of the Storø gold prospect, Godthåbsfjord region, southern West Greenland: Results of detailed mapping, structural analysis, geochronology and geochemistry. Danmarks Grønlands Geologiske Undersøgelse Rapport 2007/83, 158 pp.

Viehmann, S., Hoffmann, J. E., Münker, C., Bau, M., 2013. Decoupled Hf-Nd isotopes in Neoarchean seawater reveal weathering of emerged continents. Geology, G35014-1.

Wilton, D.H.C., 1994. Metallogenic overview of the Nain Province, northern Labrador. Canadian Institute of Mining, Metallurgy and Petroleum Bulletin 89, 43-52.

Windley, B., Garde, A.A., 2009. Arc-generated blocks with sections in the North Atlantic craton of West Greenland: Crustal growth in the Archean with modern analogues. Earth-Science Reviews 93, 1-30.

Figure captions

Fig. 1. Overview map of the Nuuk-region. The island of Storø is located in the central part of the map. Based on mapping by the Geological Survey of Denmark and Greenland (GEUS).

Fig. 2. Map of the central part of Storø. The contact between the Storø Supracrustal Belt and the Storø Anorthosite Complex is located between the layered amphibolite (unit av) and the biotite gneiss (unit b). Please note that the garnet-rich gneiss (unit grt) has been included in the biotite gneiss on this map, because it is too small to distinguish at this scale. It is for the same reason that the iron formation is also not shown in this map. Detailed geological maps of Qingaaq (Q) and Aappalaartoq (A) with all of the mapped lithological units can be found in **Appendix C** (**Figs. C1 and C2**).

Fig. 3. Photographs of various lithological units of the Storø Supracrustal Belt: a) amphibolite (unit a), b) garnet-bearing amphibolite, c) garnet-rich gneiss (unit grt), d) calc-silicate gneiss (unit f), e) biotite gneiss (unit b), f) quartzite (unit q). Pen for scale.

Fig. 4. Felsic fragments within the amphibolite (unit a), which are interpreted as being of possible volcaniclastic origin. Hammer for scale with a shaft of about 1 meter in length.

Fig. 5. Primitive mantle-normalised (Sun and McDonough, 1989) trace element diagram for lithological units of the Storø Supracrustal Belt. Most units have relatively flat trace element patterns consistent with mafic igneous protoliths and precursors, whereas the sedimentary rocks show a more evolved contribution to their incompatible element inventory. The shaded area represents the entire compositional range of these samples.

Fig. 6. Weathering index of Ohta and Arai (2007). It should be noted that even fresh rocks have W-indices slight above zero, but unaltered samples fall on the igneous fractionation trend. The amphibolites plot in the mafic corner and some of the garnet-bearing amphibolites show elevated weathering index consistent with some degree of alteration. The garnet-rich and calc-silicates gneisses are significantly more altered. The biotite gneisses show a mixed mafic-felsic source and strong weathering, and the quartzites show similar degrees of weathering, but with a larger felsic component. The origin on the mafic (M) to felsic (F) fractionation trend of the samples that are projecting away from this, indicates the approximate bulk composition of their igneous source. This suggests an intermediate source for the biotite gneisses, a felsic source for the quartzites and a mafic source for the alteration products (calc-silicate gneiss (unit ‘f’) and garnet-rich gneiss (unit grt)).

942 Fig. 7. εNd_t evolution relative to CHUR and DM. Note the large range in the initial εNd_t for the
943 samples from the Storø Supracrustal Belt at 2800 Ma, whereas samples from the Storø Anorthosite
944 Complex suggest a juvenile source at 3050 Ma.
945
946 Fig. 8. Probability density diagrams: a) biotite gneiss (KSZ-06), b) the quartzite (KSZ-13) of the
947 Storø Supracrustal Belt.
948
949 Fig. 9. Probability density diagram (a) and concordia plot (b) for the 'ag amphibolite' (KSZ-10) of
950 the Storø Anorthosite Complex.
951
952 Fig. 10. Th/Yb vs. Nb/Yb diagram (Pearce, 2008) with the MORB-OIB array outlined. All of the
953 samples from the Storø Supracrustal Belt plot above the mantle array, indicating the addition of a
954 subduction zone component or alternatively minor crustal contamination. In **Section 6.2** we argue
955 that mantle overprinting by slab of sediment melts appear more likely than AFC-processes. The
956 regional TTG field is based on data from Kokfelt (2011).
957
958 Fig. 11. Nb/Nb* and Th/Yb vs. initial εNd_t. The samples from the Storø Supracrustal Belt show
959 good correlation, which suggest some degree of contamination with a more evolve component.
960
961 **Supplementary Online Material**
962
963 Appendix A. Review of previous metamorphic, geochronological and structural work on Storø.
964
965 Appendix B. Descriptions of lithological units and detailed petrography of specific samples.

- The <2800 Ma Storø Supracrustal Belt sequence have slightly contaminated Nd-isotopes.
- Subduction zone setting with back-arc rifting forming a sedimentary basin is proposed.
- Proximal sediment source suggests significant continental freeboard by 2800 Ma.

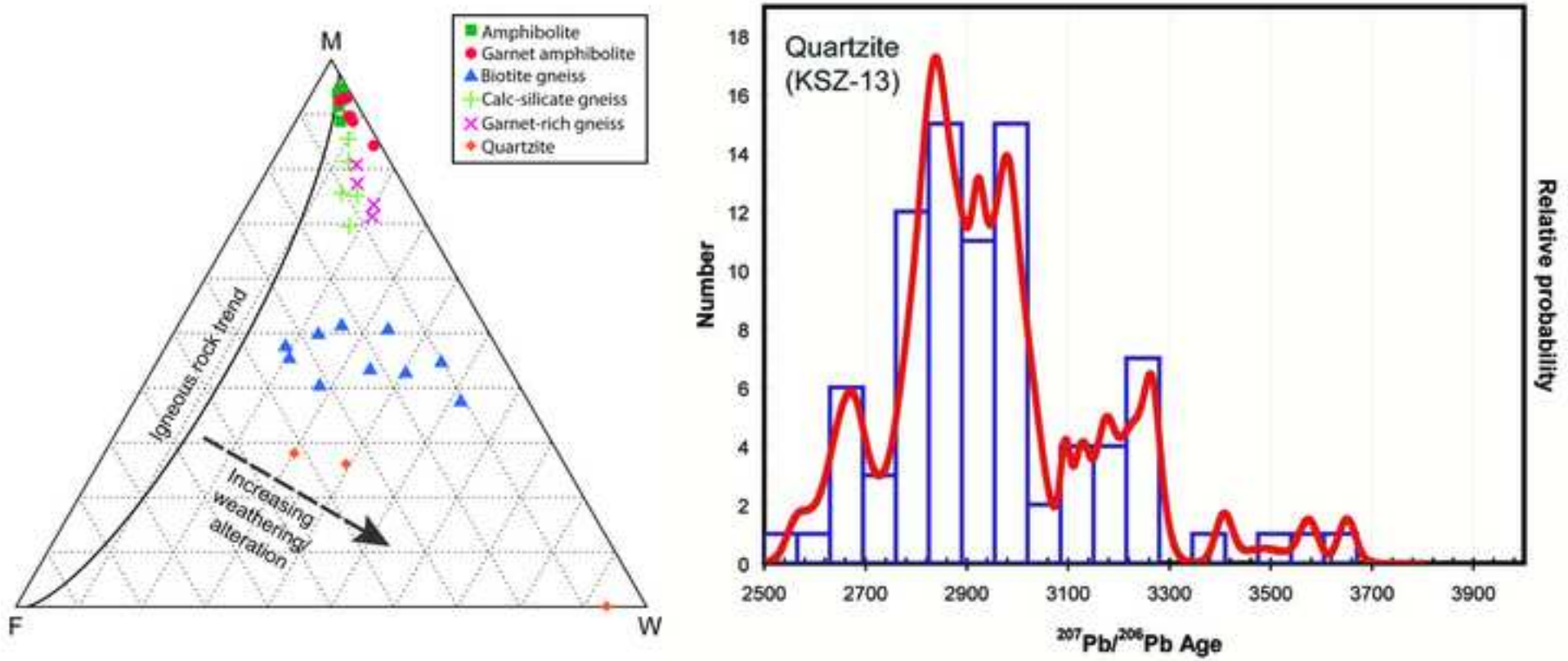
M
F
W
Amphibolite
Garnet amphibolite
Biotite gneiss
Calc-silicate gneiss
Garnet-rich gneiss
Quartzite
Igneous rock trend
Increasing weathering/ alteration
Quartzite
(KSZ-13)
Number
Relative probability
0
2
4
6
8
10
12
14
16
18
2500
2700
2900
3100
3300
3500
3700
3900
207Pb/206Pb Age

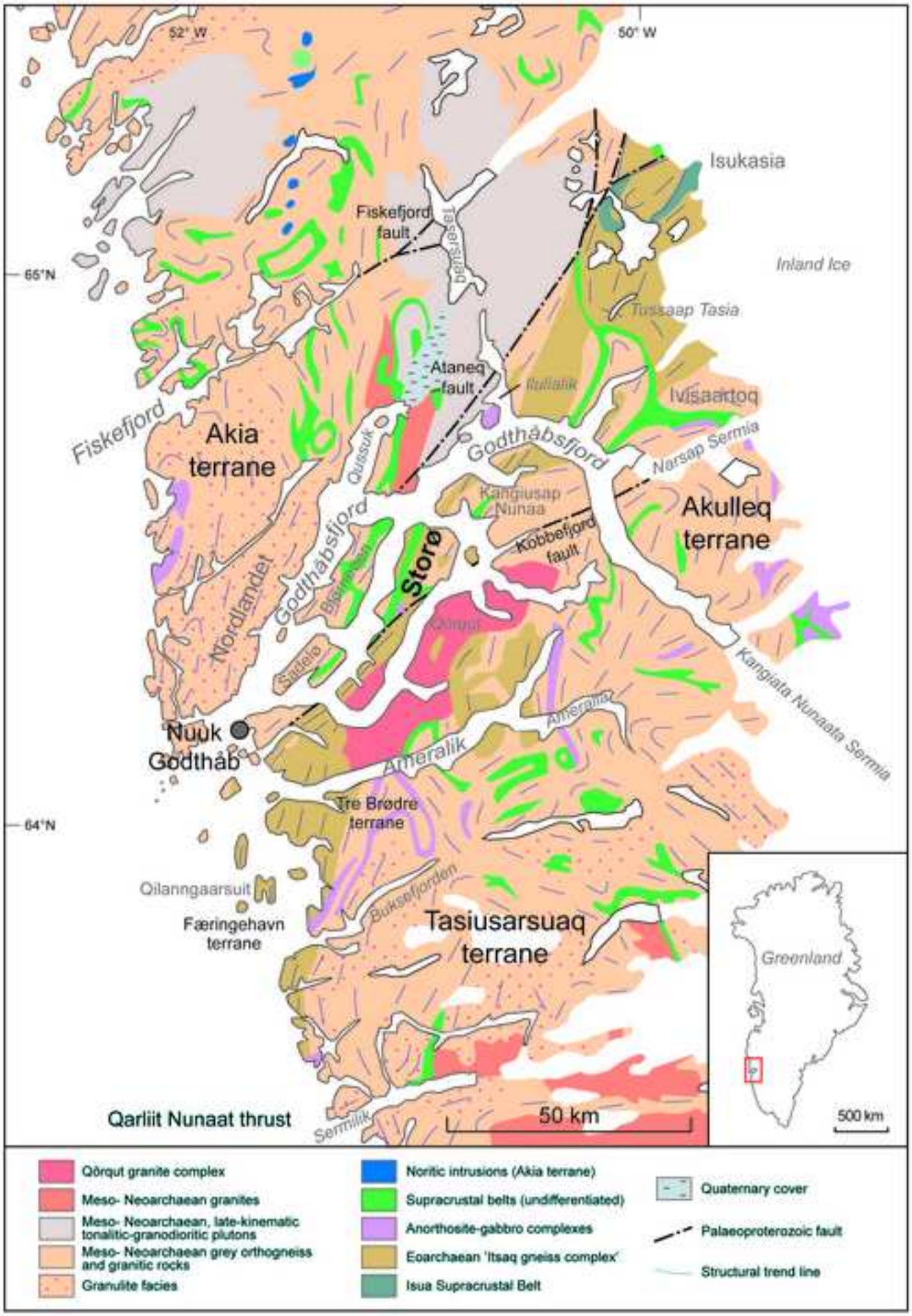

Figure 2

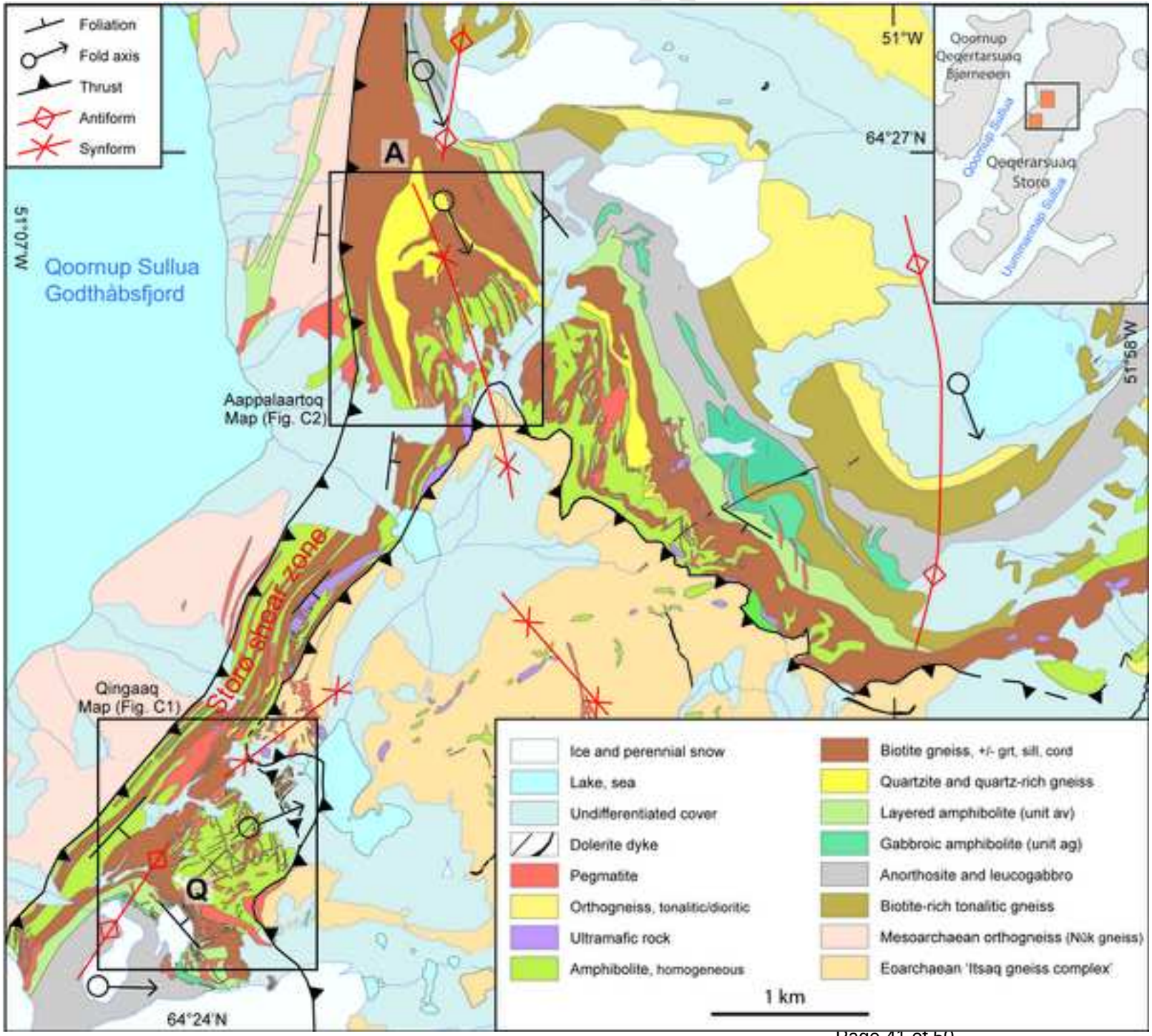
Foliation
Fold axis
Thrust
Antiform
Synform
51°W
64°27'N
51°07'W
51°58'W
64°24'N
Qoornup Sullua
Godthåbsfjord
Qoornup Qeqertarsuaq Bjerneoen
Qeqertarsuaq Store
A
Aappalaartoq
Map (Fig. C2)
Qingaaq
Map (Fig. C1)
Q
Store shear zone
Ice and perennial snow
Lake, sea
Undifferentiated cover
Dolerite dyke
Pegmatite
Orthogneiss, tonalitic/dioritic
Ultramafic rock
Amphibolite, homogeneous
Biotite gneiss, +/- grt, sill, cord
Quartzite and quartz-rich gneiss
Layered amphibolite (unit av)
Gabbroic amphibolite (unit ag)
Anorthosite and leucogabbro
Biotite-rich tonalitic gneiss
Mesoarchaean orthogneiss (Nûk gneiss)
Eoarchaean 'Itsaq gneiss complex'
1 km

Figure 4

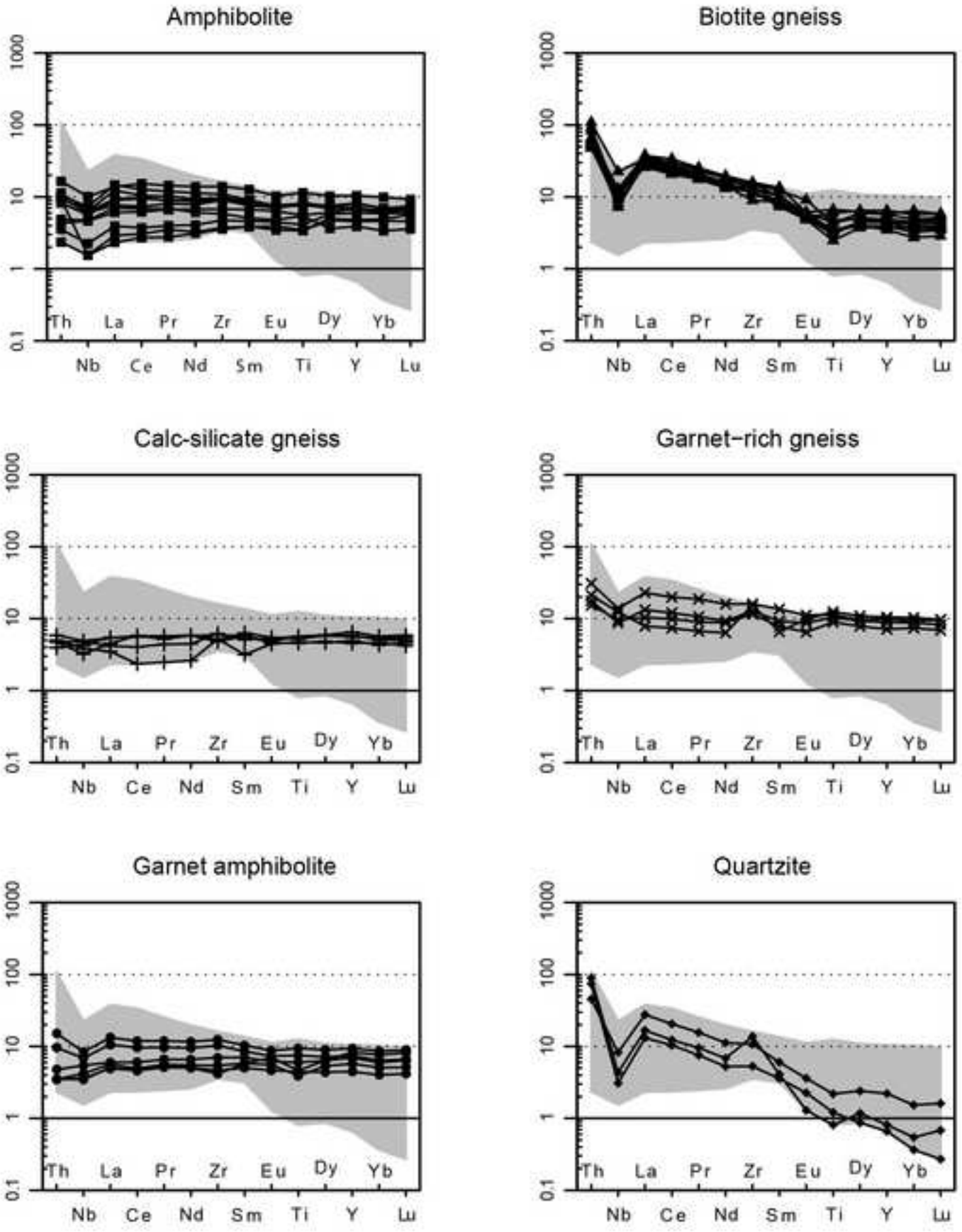

Figure 6

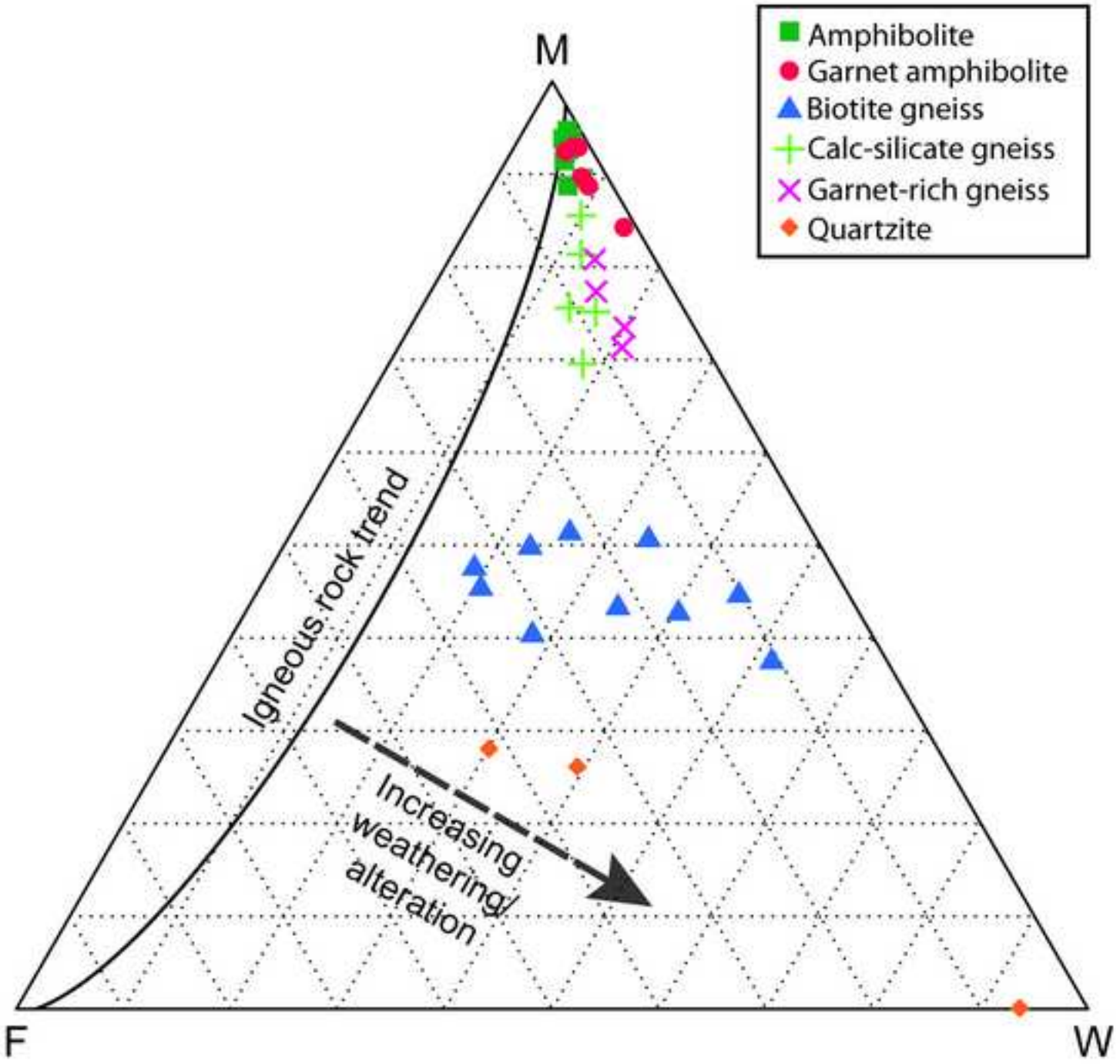
M
F
W
Amphibolite
Garnet amphibolite
Biotite gneiss
Calc-silicate gneiss
Garnet-rich gneiss
Quartzite
Igneous rock trend
Increasing weathering/ alteration

Figure 7

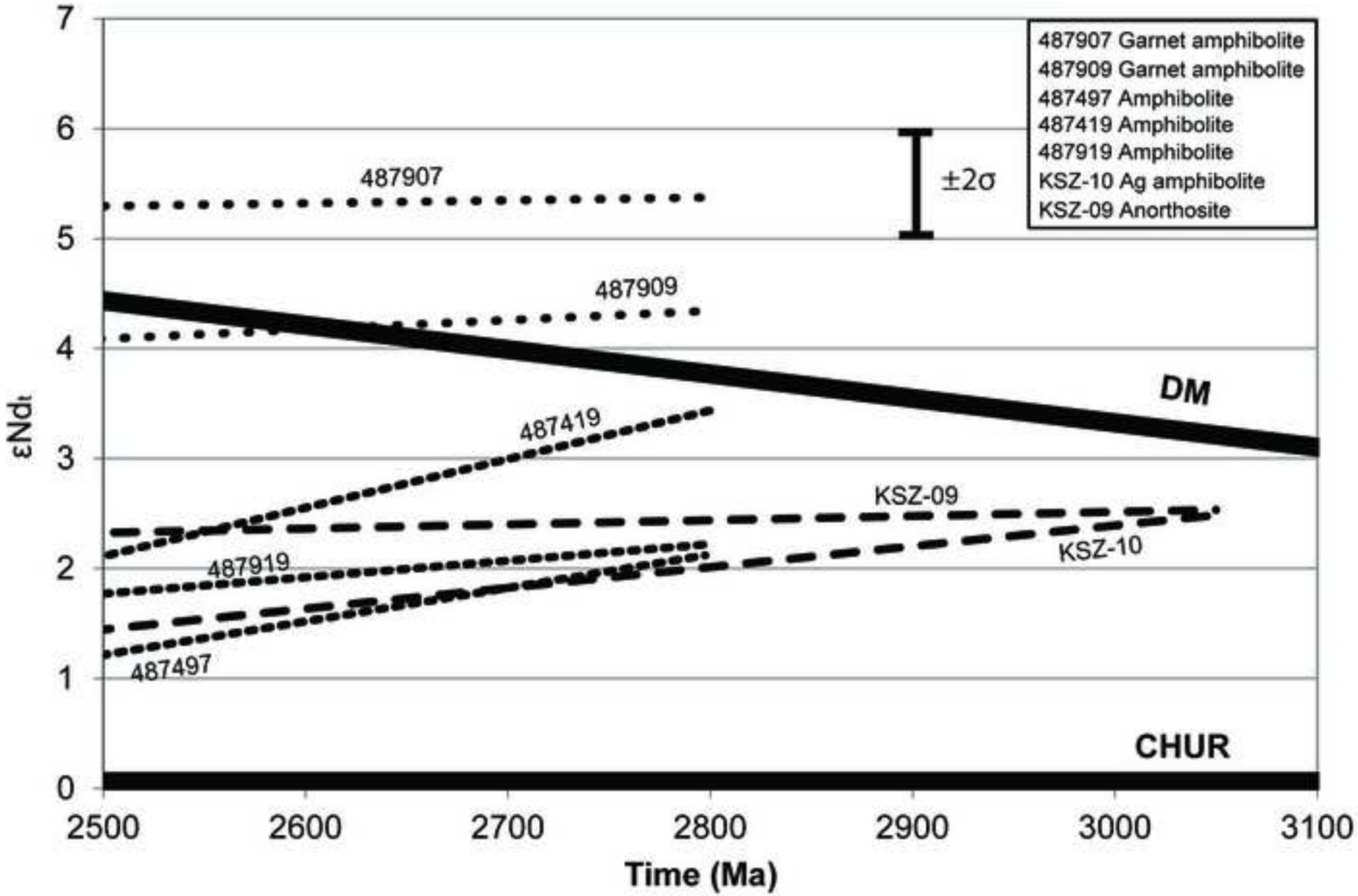
487907 Garnet amphibolite
487909 Garnet amphibolite
487497 Amphibolite
487419 Amphibolite
487919 Amphibolite
KSZ-10 Ag amphibolite
KSZ-09 Anorthosite
±2σ
487907
487909
487419
487919
487497
KSZ-09
KSZ-10
DM
CHUR
εNdt
Time (Ma)
0
1
2
3
4
5
6
7
2500
2600
2700
2800
2900
3000
3100

Figure 8

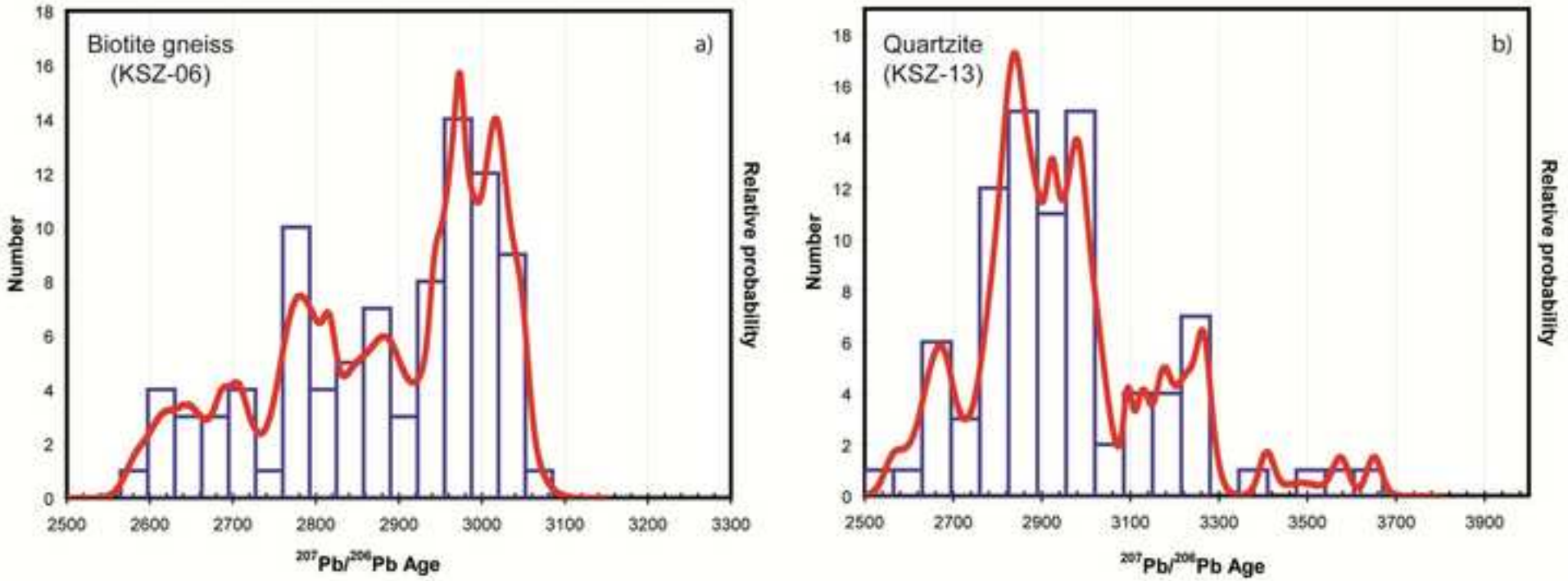
Biotite gneiss
(KSZ-06)
a)
Number
Relative probability
$^{207}Pb/^{206}Pb$ Age
Quartzite
(KSZ-13)
b)
Number
Relative probability
$^{207}Pb/^{206}Pb$ Age

Figure 9

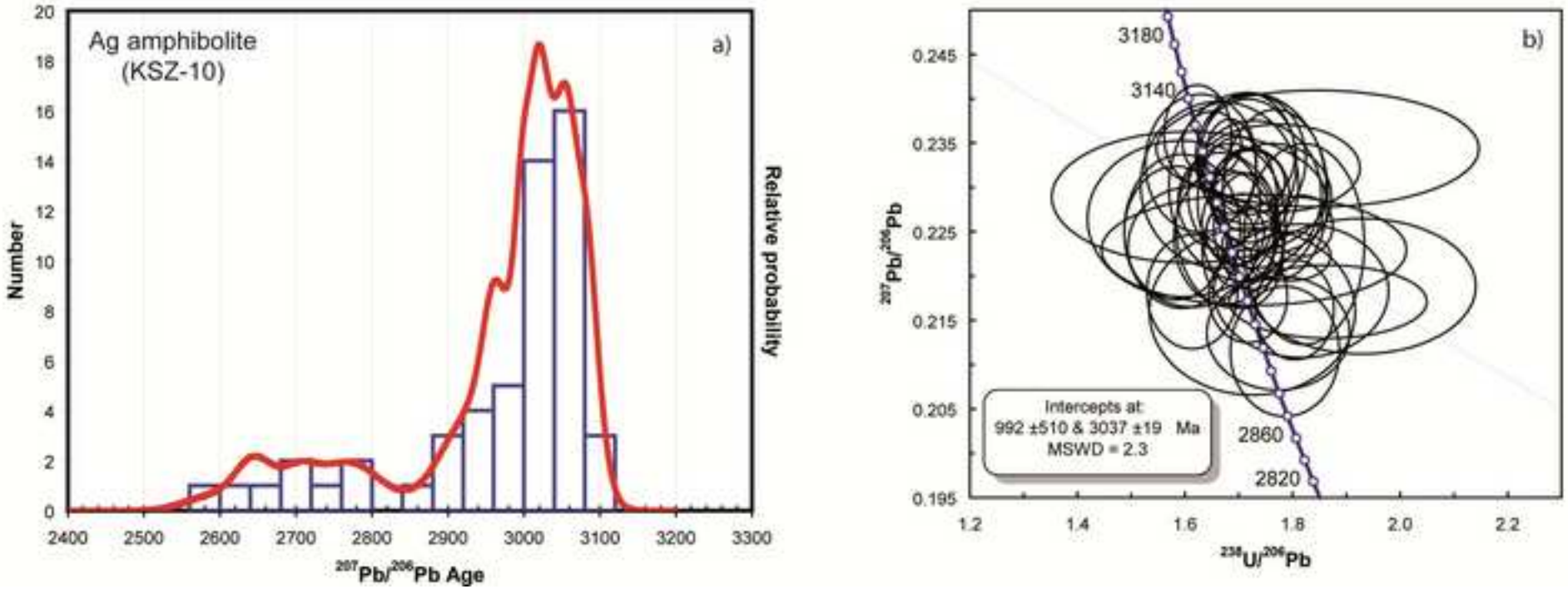
Ag amphibolite
(KSZ-10)
a)
Number
Relative probability
$^{207}Pb/^{206}Pb$ Age
b)
3180
3140
2860
2820
Intercepts at:
992 ±510 & 3037 ±19 Ma
MSWD = 2.3
$^{207}Pb/^{206}Pb$
$^{238}U/^{206}Pb$

Figure 10

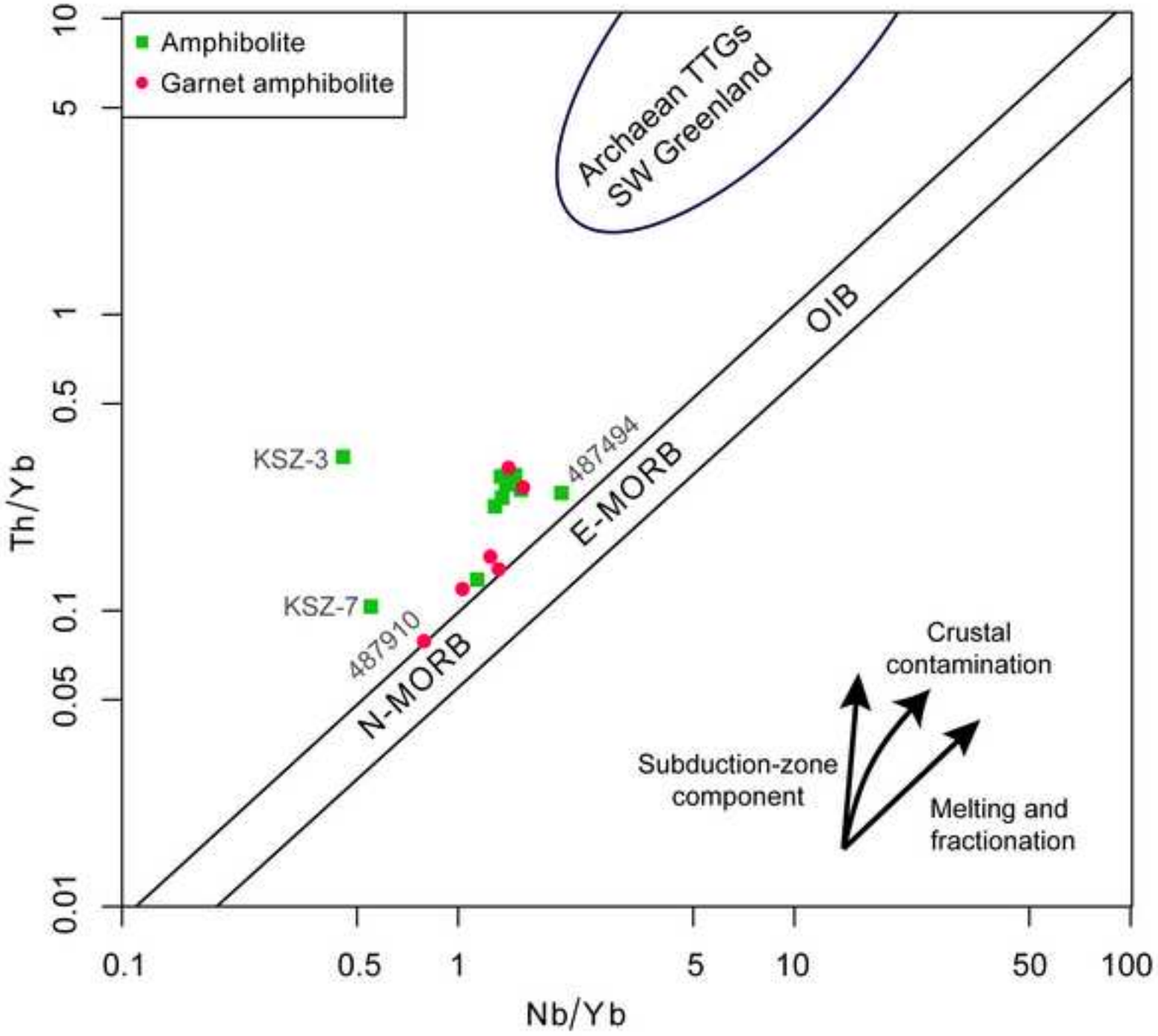
Amphibolite
Garnet amphibolite
Archaean TTGs
SW Greenland
OIB
E-MORB
N-MORB
KSZ-3
487494
KSZ-7
487910
Crustal
contamination
Subduction-zone
component
Melting and
fractionation
Th/Yb
Nb/Yb
0.01
0.05
0.1
0.5
1
5
10
0.1
0.5
1
5
10
50
100

Figure 11

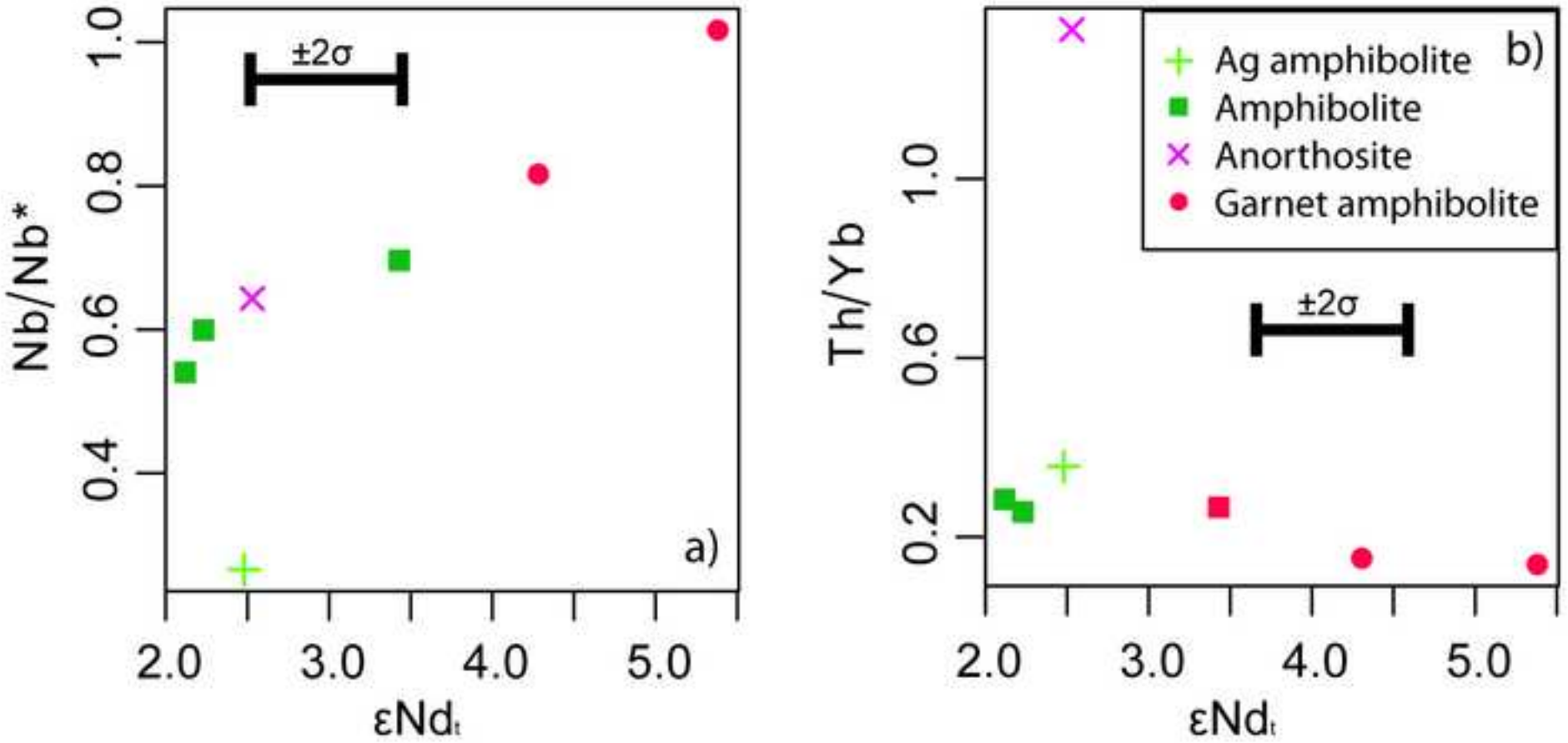
Nb/Nb*
1.0
0.8
0.6
0.4
±2σ
a)
2.0
3.0
4.0
5.0
εNdt
Th/Yb
1.0
0.6
0.2
Ag amphibolite
Amphibolite
Anorthosite
Garnet amphibolite
b)
±2σ
2.0
3.0
4.0
5.0
εNdt